

**A Computational Analysis of the Application of
Skewness and Kurtosis to Corrugated and
Abraded Surfaces**

by

© Tyler Downey

A thesis submitted to the

Department of Physics and Physical Oceanography

in partial fulfillment of the

requirements for the degree of

Masters of Science

Department of Physics and Physical Oceanography

Memorial University of Newfoundland

October 2016

St John's

Newfoundland & Labrador

Abstract

In this work, we describe the results of our investigation into the relevance of skewness and kurtosis as measures of surface roughness. Two types of surfaces are computationally generated: abraded surfaces consisting of surface scratches, and corrugated surfaces consisting of hemispherical features. It was found that abraded surfaces could be well described by the skewness and kurtosis, which can both be specified by the degree of coverage by the features on a surface. These two parameters showed a large variation over the range of surfaces sampled. The root mean squared (RMS) slope and surface area ratio did not change significantly by comparison, and the RMS roughness changed significantly only for surfaces with a large variation of scratch depths. A monotonic relationship was found to exist between skewness and kurtosis for abraded surfaces composed mainly of smaller scratches. For corrugated surfaces, the skewness and kurtosis were nearly constant for surfaces with RMS roughness values that differed significantly. The RMS roughness, RMS slope, and surface area ratio

changed significantly by comparison. No monotonic relationship was found between the skewness and kurtosis for corrugated surfaces. This indicates that corrugated surfaces are best described by the RMS roughness, RMS slope, and surface area ratio rather than the skewness and kurtosis.

Table of Contents

Abstract	iii
List of Tables	vi
List of Figures	xiii
Acknowledgments	xiv
1 Introduction	1
1.1 History of Skewness and Kurtosis	1
1.2 Other Statistical Parameters	6
1.3 Motivation	7
1.4 Previous Work	8
1.5 Scope of Thesis	10

2	Computational Details	11
2.1	Abraded Surfaces Simulations	14
2.2	Corrugated Surfaces Simulations	23
3	Results and Discussion	28
3.1	Corrugated Surfaces Results	28
3.2	Abraded Surfaces Results	42
3.3	Discussion	51
4	Conclusions	56
4.1	Future Work	60

List of Tables

1.1	Mathematical definitions of surface height statistical parameters. . . .	6
-----	--	---

List of Figures

1.1	Sample distributions with $S_{sk} > 0, S_{ku} > 3$ in blue, $S_{sk} = 0, S_{ku} = 3$ in red, and $S_{sk} < 0, S_{ku} < 3$ in green.	5
2.1	a) A sample cross-section of an abraded surface with 200 scratches with a distribution of 5%, 10%, 25%, and 60% coarse, medium, fine, and superfine scratches. b) the corresponding computer generated surface.	12
2.2	a) A sample cross-section of a corrugated surface with $a = b = c = 46$. b) the corresponding computer generated surface.	12
2.3	The primary profile a) is fitted with a weighted Gaussian function b), which results in the waviness profile. The primary profile can then be split into the roughness profile c), and the waviness profile d).	15
2.4	An example of the Graphical User Interface for the abraded surfaces simulation.	16

2.5	a) A vector diagram showing a vector \vec{r} that terminates on the line ℓ , given by Equation 2.4. b) A vector diagram that shows a vector \vec{r} that does not terminate on the line ℓ . c) A figure showing the geometric derivation of Equation 2.7.	18
2.6	A diagram of a sample surface segment at points $x_{i,j}$, $x_{i+1,j}$, $x_{i,j+1}$, and $x_{i+1,j+1}$. The surface formed by connecting the heights at each point can be divided along one diagonal into areas A_1 and A_2 or along the other diagonal into areas A_3 and A_4 . These areas are used to compute the surface area of the segment as in Equation 2.8	21
2.7	A sample distribution of surface heights for a surface composed of 200 scratches and a scratch distribution of 5%, 10%, 25%, 60% coarse, medium, fine, and superfine scratches.	23
2.8	An example of the Graphical User Interface for the corrugated surfaces simulation.	24
2.9	An example of an elliptic paraboloid. The parameters a and b control the curvature of the object, while c controls the vertical elongation.	26
2.10	A sample of the cross-section (top) and the surface height distribution (bottom) outputs from the corrugated surfaces simulation.	27

3.1	a) A computer-generated corrugated surface compared with a b) AFM image of a gold surface.	29
3.2	a) Parabolas with $c = 10$ and a ranging from $a = 10$ (red), $a = 22$ (orange), $a = 34$ (green), $a = 46$ (turquoise), $a = 58$ (blue), and $a = 70$ (violet). b) Parabolas with $a = 10$ and c ranging from $c = 10$ (red), $c = 22$ (orange), $c = 34$ (green), $c = 46$ (turquoise), $c = 58$ (blue), and $c = 70$ (violet).	30
3.3	Examples of computer-generated corrugated surfaces with varying a , along with a cross-sectional plot, and the surface height distribution for each surface. Each surface has $c = 10$ and $z_0 = 0$	30
3.4	Examples of computer-generated corrugated surfaces with varying c , along with a cross-sectional plot, and the surface height distribution for each surface. Each surface has $a = 10$ and $z_0 = 0$	31
3.5	Examples of computer-generated corrugated surfaces with varying z_0 , along with a cross-sectional plot, and the surface height distribution for each surface. Each surface has $a = 10$ and $c = 10$	32
3.6	Examples of computer-generated corrugated surfaces with a , c , and z_0 all varying.	33

-
- 3.7 a) A periodic corrugated surface without randomness. b) A zoom-in of a). Both a and NND are shown, and appear larger than they would in a). 36
- 3.8 a) Statistical parameters vs. a^* . Circles represent $c = 10$, squares represent $c = 30$, triangles represent $c = 50$, and diamonds represent $c = 70$. All data in this plot has $z_0 = 0$. b) Statistical parameters vs a^* . Circles represent $z_0 = 0$, squares represent $z_0 = 8$, triangles represent $z_0 = 16$, and diamonds represent $z_0 = 20$. All data in this plot has $c = 10$. † Several sets of data are overlapping in this plot. . . 37
- 3.9 a) Statistical parameters vs. c^* . Circles represent $a = 10$, squares represent $a = 30$, triangles represent $a = 50$, and diamonds represent $a = 70$. All data in this plot has $z_0 = 0$. b) Statistical parameters vs c^* . Circles represent $z_0 = 0$, squares represent $z_0 = 8$, triangles represent $z_0 = 16$, and diamonds represent $z_0 = 20$. All data in this plot has $a = 10$. † Several sets of data are overlapping in this plot. . . 38
-

3.10 a) Statistical parameters vs. z_0 . Circles represent $c = 10$, squares represent $c = 30$, triangles represent $c = 50$, and diamonds represent $c = 70$. All data in this plot has $a = 10$. b) Statistical parameters vs z_0 . Circles represent $a = 10$, squares represent $a = 30$, triangles represent $a = 50$, and diamonds represent $a = 60$. All data in this plot has $c = 10$	40
3.11 Kurtosis vs. skewness with RMS roughness represented with colour. The RMS roughness ranges from 0.018 (blue) to 5.83 (red).	41
3.12 Left: A sample simulated abraded surface with 200 scratches. Right: A scratched surface displayed with permission from Dr. Marko Sedlaček.	42
3.13 a) Statistical parameters for surfaces with a scratch depth distribution of 5% coarse, 5% medium, 10% fine and 80% superfine scratches. b) Kurtosis vs. skewness for this distribution.	44
3.14 a) Statistical parameters with a scratch depth distribution of 5% coarse, 10% medium, 25% fine and 60% superfine scratches. b) Kurtosis vs. skewness for this distribution.	45
3.15 a) Statistical parameters with a scratch depth distribution of 10% coarse, 20% medium, 40% fine and 30% superfine scratches. b) Kurtosis vs. skewness for this distribution.	46

3.16 a) Statistical parameters with a scratch depth distribution of 20% coarse, 40% medium, 30% fine and 10% superfine scratches. b) Kurtosis vs. skewness for this distribution. 47

3.17 a) Statistical parameters with a scratch depth distribution of 40% coarse, 30% medium, 20% fine and 10% superfine scratches. b) Kurtosis vs. skewness for this distribution. 48

3.18 A comparison of a) a cross-section of an abraded surface composed of 200 scratches distributed with a majority of smaller scratches, and b) a cross-section of an abraded surface composed of 200 scratches distributed with a majority of larger scratches. Note that the maximum scratch height in a) is approximately 0, while the maximum scratch height in b) is approximately -2 50

3.19 a) Statistical parameters for surfaces with a scratch depth distribution of 5% coarse, 10% medium, 25% fine and 60% superfine scratches, with a maximum radius of 18. Note the increase in the range of RMS roughness as compared with Figure 3.14. b) The kurtosis vs. skewness curve for the same distribution as a), for simulations conducted with maximum radii of 6 (red) and 18 (blue). 52

3.20 Kurtosis vs. skewness curves for all distributions sampled. Note that all distributions fall on a single, universal curve.	54
3.21 A comparison of a) the cross-sectional plot of a corrugated surface, and b) the inverted cross-sectional plot of an abraded surface composed of 300 scratches.	55

Acknowledgments

First and foremost, I would like to thank my supervisor, Dr. Luc Beaulieu, for guiding me along in this accelerated program, and for ensuring that I stayed on the right track with my writing and thinking. I would like to thank my friends and colleagues for their support and distraction throughout this whole program, and the Department of Physics, for providing many opportunities for me to hone my skills as both a researcher and leader. I would also like to thank Dr. Todd Andrews for keeping an eye on my progress in the early days of this program, and for making sure I was aware of the requirements and challenges of an accelerated masters program. Finally, I thank my parents; your continued support has been invaluable, and your faith in me was the main reason why I thought I could accomplish this in the first place.

Chapter 1

Introduction

1.1 History of Skewness and Kurtosis

The skewness and kurtosis are statistical parameters that were first conceptualized by Karl Pearson in 1894 and 1895 [1], [2]. In the 19th century, it was common practice among scientists to fit experimental data to a normal distribution, even in cases of large deviation from the normal distribution [3]. Noticing this, Pearson began the development of a set of functions that could be used to model distributions that deviated from the normal. This set was derived based on the use of the moments of a distribution to characterize the shape of a non-normal frequency distribution. Moments are a quantitative measure of the shape of a set of points, and are defined

as:

$$\mu_n = \frac{1}{N} \sum_{i=1}^N (z_i - \bar{z})^n, \quad (1.1)$$

where z_i are the data points, and \bar{z} is the mean of the distribution. Using this definition, Pearson defined characteristic coordinates, (β_1, β_2) , in Pearson's function space, as

$$\beta_1 = \frac{\mu_3^2}{\mu_2^3}, \beta_2 = \frac{\mu_4}{\mu_2^2}. \quad (1.2)$$

All distributions in Pearson's set can be described as a function of these coordinates; that is, all Pearson's frequency curves could be uniquely determined by their first four moments [2]. These parameters will be used to derive the skewness and kurtosis. Initially, Pearson sought to quantify the degree of asymmetry (i.e. how far the mean deviated from the mode of the data set) in a distribution by creating the skew index, χ , a precursor to the modern definition of skewness, defined as

$$\chi = \frac{\bar{z} - mode}{\sigma}, \quad (1.3)$$

where \bar{z} is the mean, σ is the standard deviation of the data set, and *mode* represents the value that appears most often in the data set. A mean shifted to the right of the

mode would give $\chi > 0$, a mean shifted to the left of the mode would give $\chi < 0$, and the case of the normal distribution ($\mu = mode$) would yield $\chi = 0$ [3]. These properties give a rudimentary idea of the skew of a distribution, however there are some flaws in this definition. For discrete distributions, such as certain types of the binomial distribution, the skew index predicts positive values of χ for distributions with the mean left of the median [4].

Another proposed measure of skewness came from Bowley in 1920, in the form

$$skew = \frac{Q_1 + Q_3 - 2m}{Q_3 - Q_1}, \quad (1.4)$$

where Q_1 and Q_3 represent the first and third quartiles, which are the 25th and 75th percentiles of the distribution respectively, and m is the median of the distribution [5]. The use of quartiles is arbitrary, however; Bowley could have chosen the 10th and 90th percentiles, for example, and still used this as a measure of skewness. Further, this measure of skewness is still susceptible to the issues faced by the skew index, given by Equation 1.3. Finally, it was found that, by cubing the difference between the data points and the mean, the failure of measure of skewness for certain discrete distributions could be prevented, and thus Pearson's original coordinate β_1 began being used as a measure of skewness in the form:

$$S_{sk} = \pm\sqrt{\beta_1} = \frac{\mu_3}{\mu_2^{3/2}} = \frac{1}{N\sigma^3} \sum_{i=1}^N (z_i - \bar{z})^3. \quad (1.5)$$

This has now become the most widely used measure of skewness.

In 1895 Pearson created the concept of excess, ϵ , the precursor to kurtosis [2], defined as

$$\epsilon = \frac{\mu_4 - 3\mu_2^2}{3\mu_2^2}. \quad (1.6)$$

In 1902, Pearson determined that ϵ measures the degree of peakedness of a distribution compared to the normal distribution [6]. If $\epsilon > 0$, then $\mu_4 > 3\mu_2^2$ and the curve is sharper than the normal distribution, and is called leptokurtic. If $\epsilon < 0$, then $\mu_4 < 3\mu_2^2$ and the distribution is flatter on top than the normal distribution, and is called platykurtic. Finally, a curve with $\epsilon = 0$ implies $\mu_4 = 3\mu_2^2$, (called mesokurtic) and is a necessary condition for the normal distribution. In terms of the parameter β_2 , we have

$$\begin{aligned} \epsilon &= \frac{\mu_4 - 3\mu_2^2}{\mu_2^2} \\ &= \frac{\mu^4}{\mu_2^2} - 3 \\ &= \beta_2 - 3, \end{aligned} \quad (1.7)$$

thus giving the modern definition for kurtosis as β_2

$$\beta_2 = S_{ku} = \frac{1}{N\sigma^4} \sum_{i=1}^N (z_i - \bar{z})^4. \quad (1.8)$$

We see that for $\chi = \epsilon = 0$, we must have $S_{sk} = 0$ and $S_{ku} = 3$. It is important to note, however, that these conditions are simply necessary conditions for the normal distribution, and are not sufficient to guarantee that a distribution is normal [3]. Sample distributions with various values of skewness and kurtosis are shown in Figure 1.1.

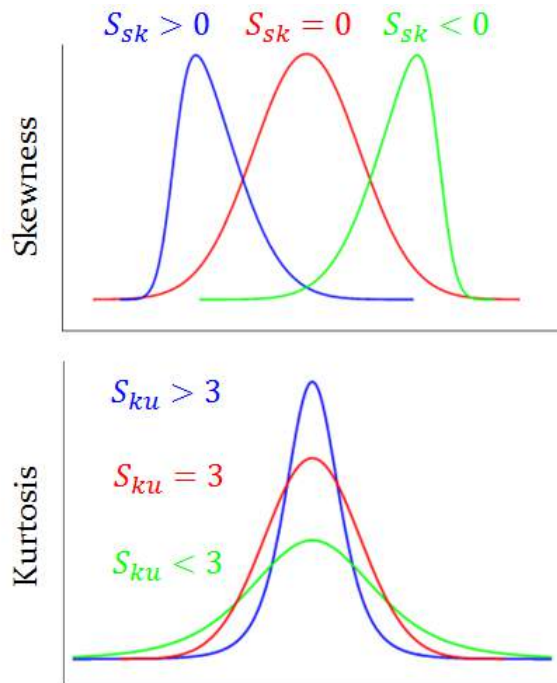


Figure 1.1: Sample distributions with $S_{sk} > 0, S_{ku} > 3$ in blue, $S_{sk} = 0, S_{ku} = 3$ in red, and $S_{sk} < 0, S_{ku} < 3$ in green.

Table 1.1: Mathematical definitions of surface height statistical parameters.

Name	Symbol	Equation
Root Mean Square Surface Height (RMS)	S_q	$\sqrt{\frac{\sum_{i=1}^N (z_i - \mu_z)^2}{N}}$
Surface Area Ratio	S_{dr}	$\frac{A_{samp} - A_{sub}}{A_{sub}} \times 100\%$
RMS Surface Slope	S_{dq}	$\left(\frac{1}{(M-1)(N-1)} \sum_{j=2}^N \sum_{i=2}^M \left[\left(\frac{z(x_i, y_j) - z(x_{i-1}, y_j)}{\Delta x} \right)^2 + \left(\frac{z(x_i, y_j) - z(x_i, y_{j-1})}{\Delta y} \right)^2 \right] \right)^{\frac{1}{2}}$

1.2 Other Statistical Parameters

In this thesis, we will also make use of three other statistical parameters: the root mean square (RMS) roughness, the RMS slope, and the surface area ratio, all defined mathematically in Table 1.1 [7]. Each of the statistical parameters described will be calculated using the surface heights of a given surface.

These parameters will be used for comparison with our results pertaining to skewness and kurtosis. Note that the RMS roughness is simply the standard deviation of the distribution, σ and measures the spread of the data. The RMS roughness is the most common measure of surface roughness, and is the most widely cited measure in the literature due to its capacity to correlate well with physically measurable roughness

effects [8–12]. The RMS slope is the root mean square of all local slopes of the surface under study, and often correlates strongly with the RMS roughness, due to the similarities in their calculation. The surface area ratio is the quotient of the area of the surface compared to the area of the underlying substrate. This quantity also increases with surface roughness, because as the local surface slopes increase, the surface features become more pronounced, thus increasing the area of the surface while the area of the substrate remains the same.

1.3 Motivation

Due to the miniaturization of components, interest in surface characterization has increased in recent years [10]. Accurate description of the roughness of a surface is a significant challenge in surface characterization, and many practical systems could benefit from a deeper understanding of surface roughness. One such example, pertinent to our research group, involves silicon microcantilevers coated with a gold film. We wish to determine the relationship between the deflection of these cantilever sensors and the surface roughness of the underlying gold film. Understanding this relationship could greatly improve the design of these sensors, ultimately leading to actual applications. Many other examples of practical uses for accurate roughness

description come from fields such as tribology, the study of relationships between surface roughness and physical parameters such as friction, wetting, and wear. Another field which makes frequent use of surface roughness measures is dental science. Typical problems in dental science include determining how abrasions on teeth affect oral health in humans, as well as how knowledge of surface roughness can help optimize denture design [13].

1.4 Previous Work

The skewness and kurtosis are used extensively in the literature. Peltonen *et al.* used them to successfully characterize the surfaces of chemically prepared sol-gel samples with different topographies [8]. Sedlacěk *et al.* used these parameters to measure the coefficient of friction of metal surfaces composed of scratches with similar RMS roughnesses, but with different skewness and kurtosis, both computationally [9], and experimentally [10]. Tayebi *et al.* modelled scratched surfaces using the Pearson system of frequency curves to predict the behaviour of the coefficient of static friction with skewness and kurtosis [11]. Hansson *et al.* investigated the effect of surface roughness on the bone response to dental implants [12], while Meierles *et al.* studied the characterization of wear in teeth [13]. Wang *et al.* investigated the effect of

skewness and kurtosis on various contact parameters of computationally generated non-Gaussian surfaces [14]. İközler *et al.* found a correlation between the skewness and kurtosis and the structure of an array of ZnO nanorods [15]. The majority of these studies were successful in correlating these statistical parameters to the physical parameters under study, with only Meireles *et al.* [13] finding the skewness to be ineffective.

The work presented in this thesis is based on a program written by Dr. Luc Beaulieu to simulate corrugated surfaces composed of hemispherical grains. These surfaces are of interest to our group because they represent the surface of a gold-coated microcantilever sensor well. Peter Martin, a B. Sc. Honours student in our group, used Dr. Beaulieu's code to attempt to correlate skewness, kurtosis and RMS roughness with surface roughness for corrugated surfaces. Martin found that corrugated surfaces with different amounts of peak height variation could have similar values for skewness and kurtosis [16]. Neither the skewness nor the kurtosis gave any indication of the sharpness or broadness of the surface features. From Martin's work, it is unclear whether the kurtosis and skewness are able to be used for characterizing surfaces [16]. However, Martin did not generate a large number of surfaces, nor did he vary the input parameters greatly, and thus the scope of this project was limited. More data and a deeper analysis are required to make a more definite statement about

the correlation of skewness and kurtosis to surface roughness.

1.5 Scope of Thesis

Although there are many studies on the applicability of the skewness and kurtosis to physical systems, apart from Martin's work there are no studies examining the surface roughness of corrugated surfaces using these two parameters. In this thesis, we will investigate, using Dr. Beaulieu's code, computationally generated corrugated surfaces more deeply. In addition, since the majority of the literature has focused on abraded surfaces composed of scratches, I have written another program to generate abraded surfaces and computed the skewness and kurtosis of these surfaces to compare with the results from those of corrugated surfaces. In this way, we hope to determine if the skewness and kurtosis are truly applicable to corrugated surfaces composed of hemispherical grains. Chapter 2 will consist of a detailed description of both the abraded and corrugated surfaces simulations, the presentation of the results and analysis of the output of the two programs will be presented in Chapter 3, and our conclusions and their implications for the study of surface characterization will be given in Chapter 4.

Chapter 2

Computational Details

Two programs were written for this study; one, written by the author, simulates abraded surfaces composed of half-cylindrical scratches, while the other, written by Dr. Luc Beaulieu and modified by the author, simulates corrugated surfaces composed of hemispherical grains. A sample of an abraded surface and cross-section can be seen in Figure 2.1, while a sample of a corrugated surface and cross-section can be seen in Figure 2.2

Both programs compute the skewness and kurtosis, as well as the RMS roughness, RMS slope, and surface area ratio for each surface type, allowing a comparison of the results for both types to be performed. Examples of abraded surfaces found in the literature are typical surfaces examined in tribological and dental science appli-

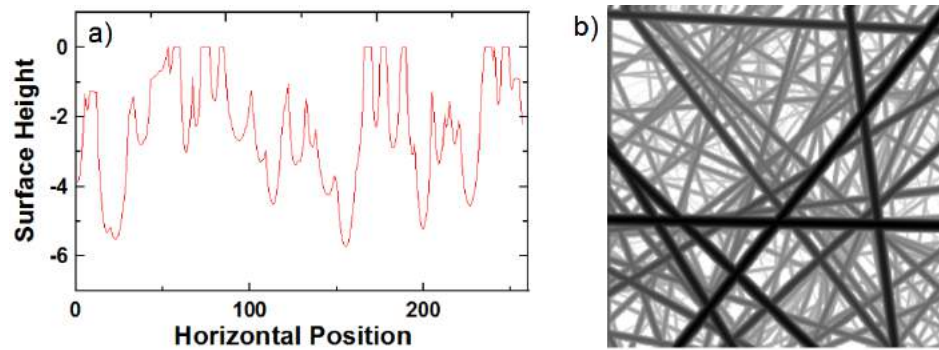


Figure 2.1: a) A sample cross-section of an abraded surface with 200 scratches with a distribution of 5%, 10%, 25%, and 60% coarse, medium, fine, and superfine scratches. b) the corresponding computer generated surface.

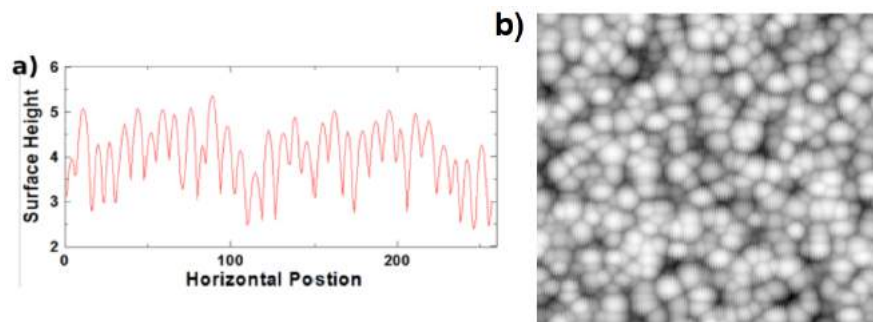


Figure 2.2: a) A sample cross-section of a corrugated surface with $a = b = c = 46$. b) the corresponding computer generated surface.

cations, as discussed in the Introduction. Additionally, the gold film deposited on a microcantilever sensor is an example of a corrugated surface. Thus, these two surface types are of interest in our research. Both programs were written using Microsoft Visual Basic, and consist of a Graphical User Interface (GUI) for both the input, and the code itself.

In order to compute the previously mentioned roughness parameters, the surface

height data (called the primary profile) must be filtered to separate its waviness and roughness profiles. This separation is standard practice in characterizing actual surfaces, and is done to account for any directionality imparted to the surface during the roughing process. This is achieved through the convolution of a 2-dimensional matrix representing the surface heights with a matrix whose entries are points in the Gaussian weighting function, given by [17]

$$G_{ij} = \frac{1}{\alpha\lambda} e^{-\pi\left(\frac{z_{ij}}{\alpha\lambda}\right)^2}, \quad (2.1)$$

where $\alpha = 0.4697$ is a constant, λ is the cut-off wavelength, chosen based on industry standards to best fit the moving average to the surface, and z_{ij} is the surface height at point (i, j) . Convolution of these matrices can be thought of as a moving average along the surface with Gaussian weights; this weighted average is the waviness profile. Matrix convolution is most easily achieved through the use of the Convolution Theorem,

$$X * Y = \mathcal{F}^{-1}(\mathcal{F}(X) \cdot \mathcal{F}(Y)) \quad (2.2)$$

where X and Y are complex-valued matrices of equal rank, the $*$ operator denotes convolution, the \cdot operator denotes term-by-term complex multiplication, \mathcal{F} denotes

the Fourier Transform, and \mathcal{F}^{-1} denotes the inverse Fourier Transform. Code written in-house which performs the Fast Fourier Transform and Inverse Transform was used to perform the convolution to obtain the waviness profile. The roughness profile, R , is, then, simply the difference between the primary profile, P , and the waviness profile, h ,

$$R = P - h. \quad (2.3)$$

Figure 2.3 shows a visual representation of this filtering process. Figure 2.3a shows a sample 2D primary profile which is fit with the moving average as discussed above. The result is shown in Figure 2.3b. Filtering the primary profile results in the roughness profile, shown in Figure 2.3c and the waviness profile, Figure 2.3d. The roughness profile, which can be thought of as the primary profile with any directionality removed, is then used to calculate the roughness parameters.

2.1 Abraded Surfaces Simulations

An image of the GUI for the abraded surfaces simulation can be seen in Figure 2.4. From this interface, the user can define values for the resolution (size of the grid to be used), G , the number of scratches for any given surface, the maximum depth of

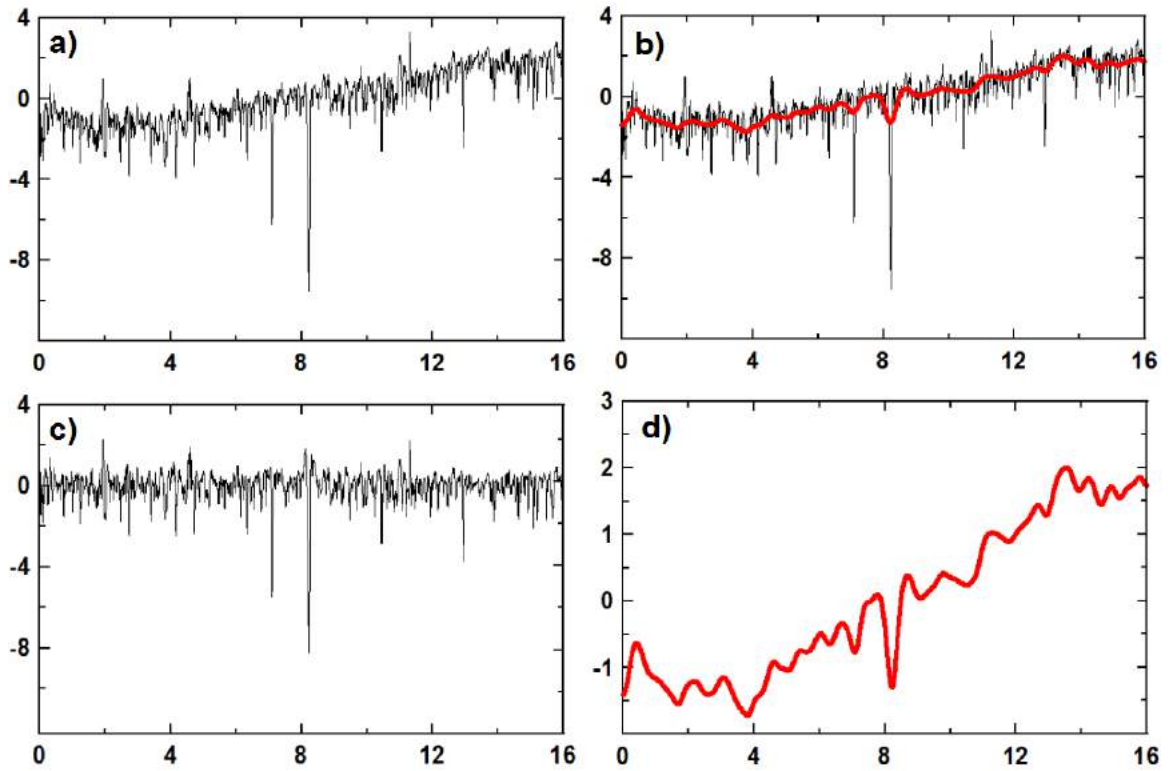


Figure 2.3: The primary profile a) is fitted with a weighted Gaussian function b), which results in the waviness profile. The primary profile can then be split into the roughness profile c), and the waviness profile d).

a scratch in the simulation, and the distribution of scratch sizes. The user can also view an image of the surface, the cross-section through the centre of the surface, and the distribution of surface heights, once a surface has been generated. The user can save the output and distribution files from the GUI as well.

The program begins by defining a two-dimensional array of size $(G + \frac{G}{10} \times G + \frac{G}{10})$, with $G = 256$ in our simulations, to represent a Cartesian grid. The $\frac{G}{10}$ border is

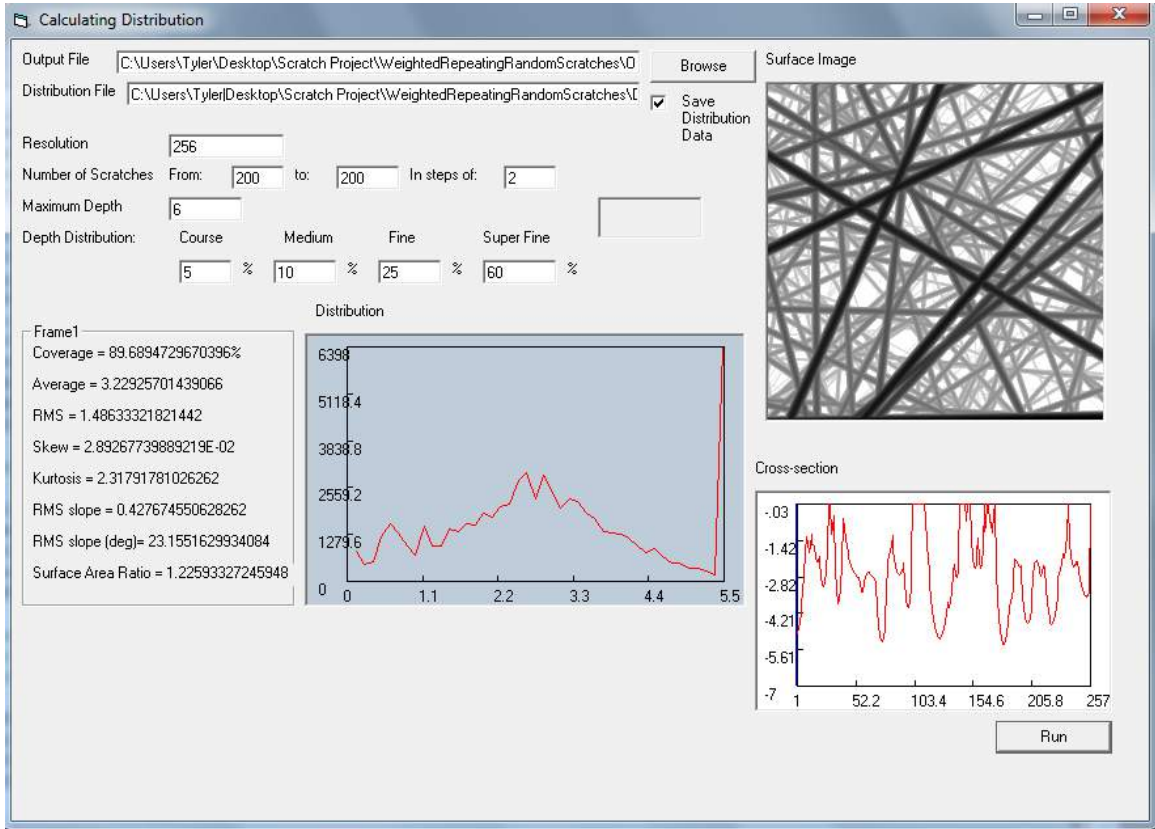


Figure 2.4: An example of the Graphical User Interface for the abraded surfaces simulation.

included to prevent edge effects and is later removed, creating a $G \times G$ surface. The array is then initialized with $z = 0$ values. To define a scratch, the equation of a line in point-normal form is used,

$$\vec{N} \cdot (\vec{r} - \vec{p}) = 0, \quad (2.4)$$

where \vec{p} is a point on the line ℓ which we wish to draw on the grid, $\vec{r} = (x, y, 0)$ is a

point on the grid, and \vec{N} is a vector normal to ℓ . Figure 2.5 a) shows, pictorially, how Equation 2.4 generates a line in a plane. The components of \vec{p} and \vec{N} are generated through the use of a random number generator. This ensures a degree of randomness in the scratch direction and placement, to more closely represent actual surfaces. The following equation was used to generate a random number, a , within upper and lower bounds, a_+ and a_- respectively:

$$a = (a_+ - a_-) \times Rnd + a_-, \quad (2.5)$$

where Rnd generates a random number between 0 and 1. Once the components of \vec{p} and \vec{N} are determined, the program uses Equation 2.5 to generate a random value for the scratch radius, ρ , within the bounds of the appropriate scratch type, and calls a function which reads in \vec{p} , \vec{N} , and ρ . The function then loops over the whole array and places a value equal to z at all points \vec{r} in the array that satisfy Equation 2.4. The set of points satisfying Equation 2.4 forms a line on the grid, which we will call ℓ , defined by \vec{N} and \vec{p} . The line, ℓ , runs axially along the scratch as shown in Figures 2.5 a and b, and will be used as a starting point for the construction of the half-cylindrical scratch.

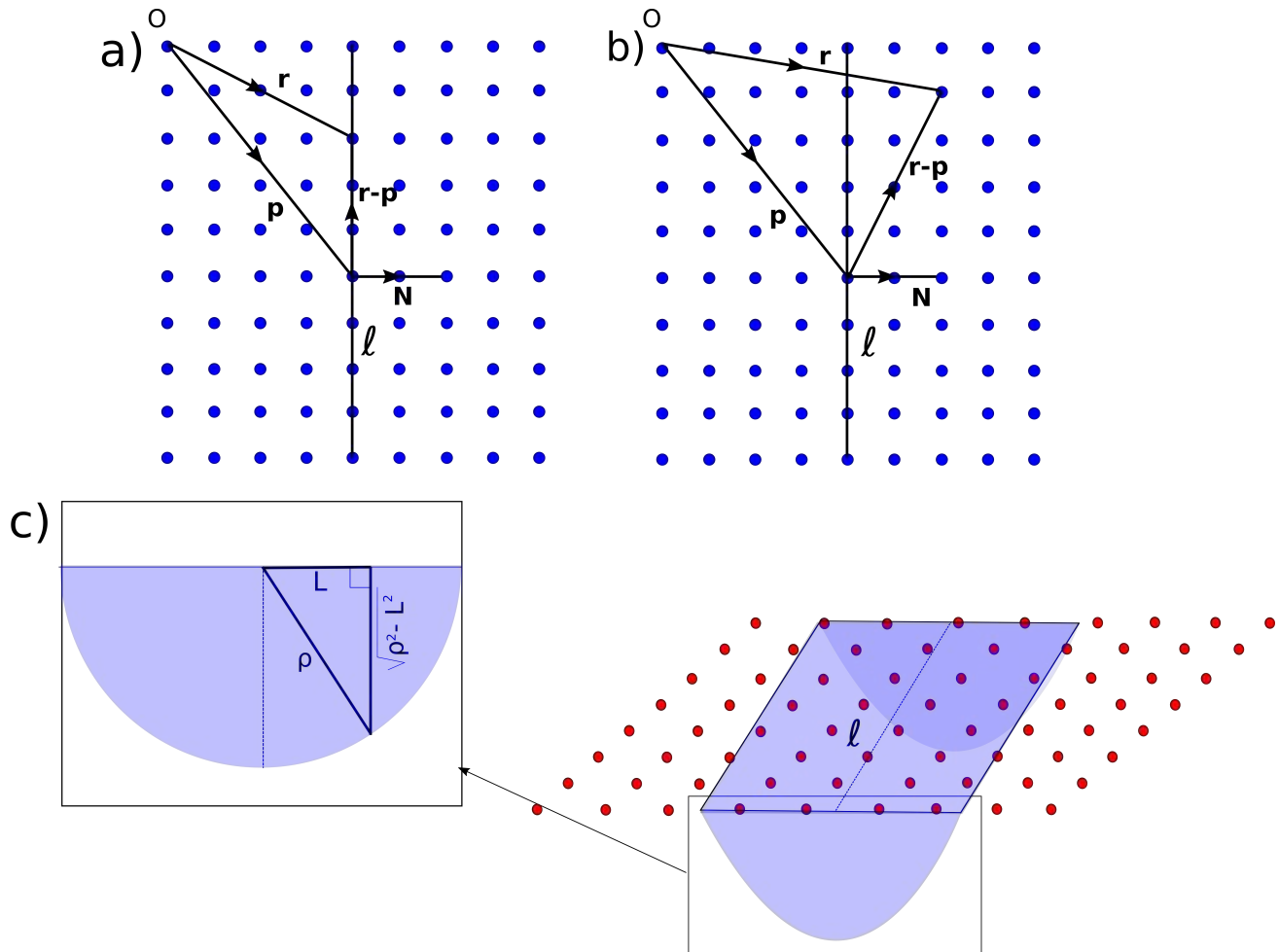


Figure 2.5: a) A vector diagram showing a vector \vec{r} that terminates on the line ℓ , given by Equation 2.4. b) A vector diagram that shows a vector \vec{r} that does not terminate on the line ℓ . c) A figure showing the geometric derivation of Equation 2.7.

To draw the half-cylinder, the program loops over the whole array and computes the in-plane perpendicular distance, L , of each vector \vec{r} as [18]

$$L = \frac{\vec{N} \cdot (\vec{r} - \vec{p})}{\|\vec{N}\|}. \quad (2.6)$$

The code then checks that $L \leq \rho$, the radius of the scratch. If false, then the point lies outside of the cylinder. If true, then the surface depth at \vec{r} is computed using:

$$z = \sqrt{\rho^2 - L^2}. \quad (2.7)$$

This equation can be derived from geometrical considerations, and is illustrated in Figure 2.5c. From the previously shown Figure 2.1a, it is clear that this equation does generate half-cylinders in the plane. The code repeats this process for the number of scratches requested, ensuring, at the intersection of multiple scratches, to always retain the lowest of the intersecting values; the result is a simulated scratched surface, as shown in Figure 2.1b.

The program also has an option for creating a distribution of scratches with different depths. Prior to using the scratch creation algorithm, the percent distribution of scratch depths is read and multiplied by the total number of scratches to get the number of each type of scratch used in the simulation. The scratch types described in this work are classified based on radius, and are, in order of decreasing radius, coarse, C , medium, M , fine, F , and superfine, SF . The scratch types are defined

based on the largest scratch depth (equal to the radius) for the surface, ρ_{max} , as $0 \leq r_{SF} < \frac{d}{4} \leq r_F < \frac{d}{2} \leq r_M < \frac{3d}{4} \leq r_C \leq d$. Note that the depth of a scratch is a continuous variable. The program inputs the number of each scratch in the surface, thus creating a surface composed of scratches with a user-defined radius distribution.

Once a number of scratches is set, the program is looped 10 times to create 10 surfaces using the same starting parameter plus random fluctuations. The statistical roughness parameters are then averaged and written to a file. The parameters S_q , S_{sk} , S_{ku} , and S_{dq} are computed using the equations given in Sections 1.1 and 1.2. The calculation of S_{dr} is done by first considering the surface heights, $z(x_{i,j})$, at grid points $x_{i,j}$, $x_{i+1,j}$, $x_{i,j+1}$, and $x_{i+1,j+1}$. Connecting these grid points forms a square in the grid, and connecting the surface heights forms triangles, depending on the values of the $z(x_{i,j})$ used, as shown in Figure 2.6. The shape is divided into triangles of area A_{ij} by dividing along both diagonals, again as shown in Figure 2.6. These areas are averaged as follows,

$$SA_{ij} = \frac{(A_1 + A_2) + (A_3 + A_4)}{2}. \quad (2.8)$$

This procedure is repeated for all (i, j) until the surface area of each segment of the surface is calculated. These areas are then summed over the surface, and the surface

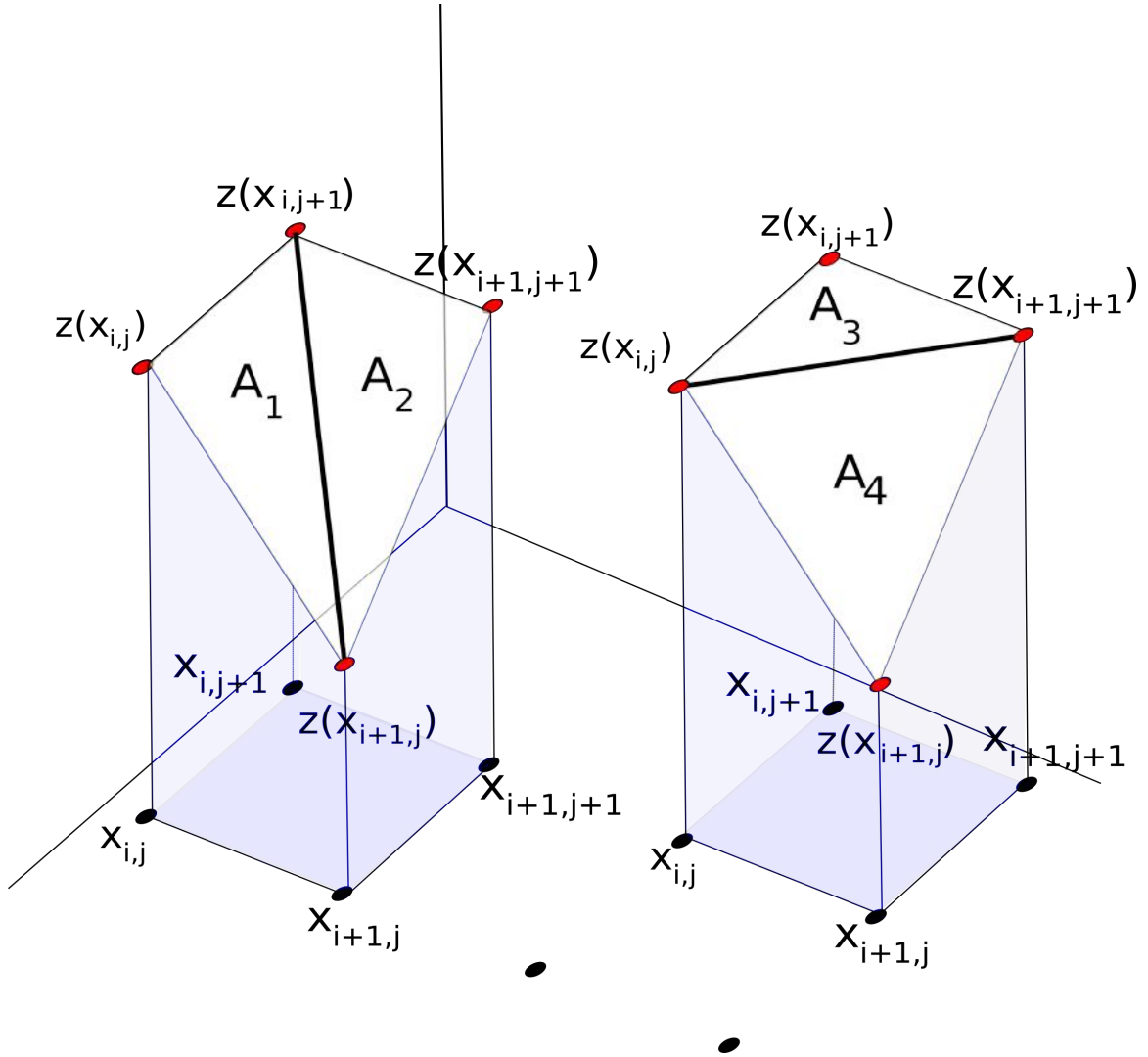


Figure 2.6: A diagram of a sample surface segment at points $x_{i,j}$, $x_{i+1,j}$, $x_{i,j+1}$, and $x_{i+1,j+1}$. The surface formed by connecting the heights at each point can be divided along one diagonal into areas A_1 and A_2 or along the other diagonal into areas A_3 and A_4 . These areas are used to compute the surface area of the segment as in Equation 2.8

area ratio, γ , is computed as

$$SA_{tot} = \sum_{i=1}^G \sum_{j=1}^G SA_{ij}, \quad (2.9)$$

$$\gamma = \frac{SA_{tot}}{G^2}.$$

To create the distribution, Scott's Rule, shown below, is used to calculate bin widths, h [19]

$$h = \frac{3.5S_q}{N^{1/3}}, \quad (2.10)$$

and, consequently, the number of bins, b ,

$$b = \frac{S_{max} - S_{min}}{h}, \quad (2.11)$$

where S_{max} and S_{min} are the surface height maximum and minimum respectively.

The program then counts the number of points that fall within each bin. A sample distribution is displayed in Figure 2.7.

All data is written to a file, as well as plotted in the GUI as shown in Figure 2.4.

Displaying the surface is accomplished by using a grayscale based on the surface height value to denote low (black) and high (white) values. Finally, to create a cross-sectional plot, the points, $(x_{(i,j=\frac{G}{2})}, z)$ along the centreline of the grid are plotted.

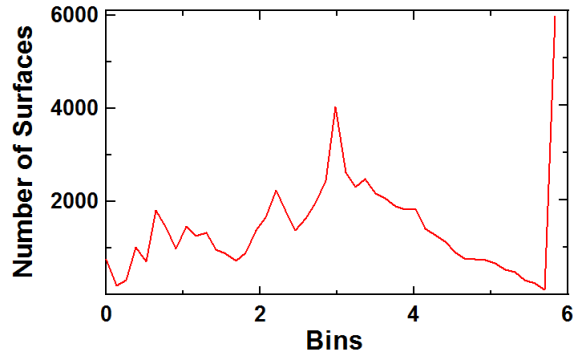


Figure 2.7: A sample distribution of surface heights for a surface composed of 200 scratches and a scratch distribution of 5%, 10%, 25%, 60% coarse, medium, fine, and superfine scratches.

2.2 Corrugated Surfaces Simulations

For this project, code written by Dr. Luc Beaulieu was used in conjunction with our abraded surfaces simulator. This was done to compare results for different surfaces to better understand the effect of surface type on the applicability of skewness and kurtosis. An example of the GUI for the corrugated surfaces simulation can be seen in Figure 2.8.

Similarly to the abraded surfaces GUI, the surface resolution, G (along with a boundary defined similarly as in the abraded surfaces code) and control parameters are defined on the interface, however for this program, the control parameters are the elliptic parameters a , b , c , and z_0 , given by the equation for an elliptical paraboloid,

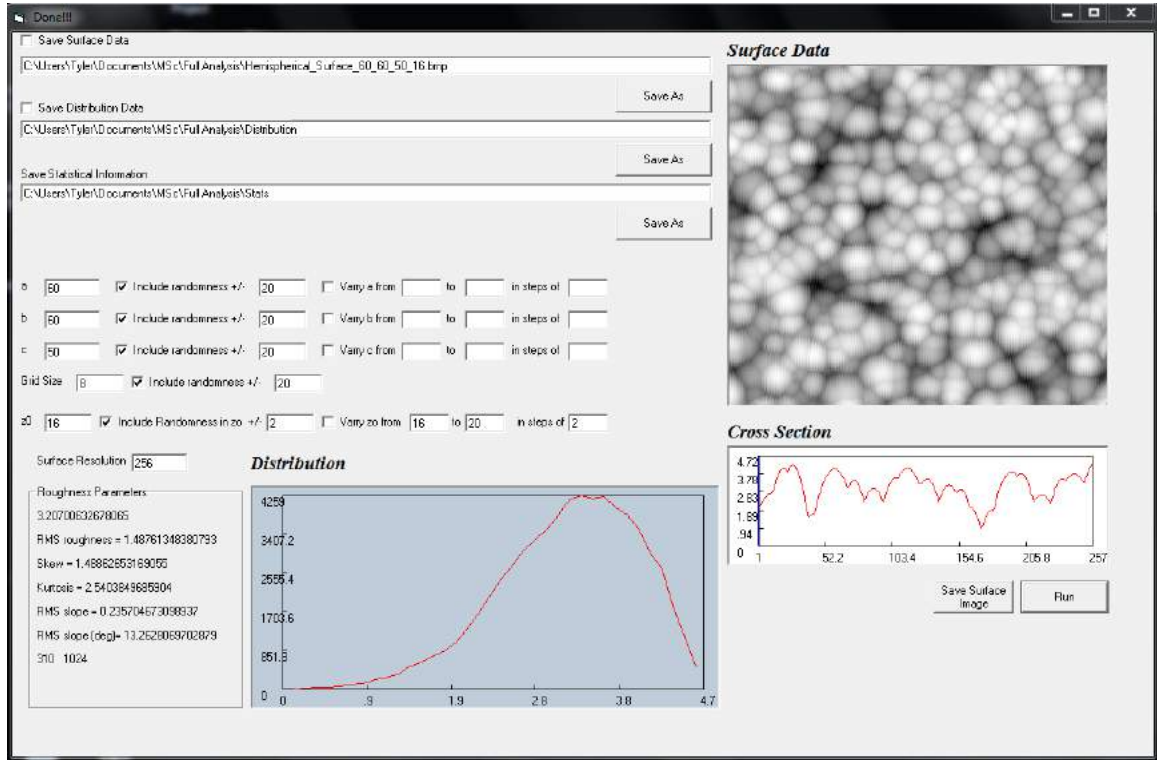


Figure 2.8: An example of the Graphical User Interface for the corrugated surfaces simulation.

$$z = c \left(\frac{(x - x_0)^2}{a^2} + \frac{(y - y_0)^2}{b^2} \right) + z_0, \quad c < 0. \quad (2.12)$$

The grid size, which we will call g , is also a control parameter for these simulations. The parameters a , and b control the curvature of the feature in the x and y directions, c controls the vertical elongation, and z_0 sets the base height of the paraboloid. Equation 2.12 is used to calculate the height of the surface features. Note that we have defined $c < 0$ to ensure that all surface features are convex on the surface. In

addition to these parameters, the statistical parameters, once computed, were written to the GUI. The surface image and plots of the cross-section and distribution are also visible on the interface. Options for saving the various data files are also available.

The algorithm for this program is described below

First, points (x_0, y_0) are defined to form a square grid to represent the centre point of a hemispherical surface feature. The grid position indices, i and j , are declared and set to loop from $\frac{g}{2}$ to $G + 2 * border - \frac{g}{2}$ in steps of g , where $border$ is the length of the border around the surface. The points (x_0, y_0) were allowed to fluctuate up to a given percentage p (usually 20%) using the equation,

$$a = a_0 + \left(\frac{a_0 * p}{100}\right) - 2\left(\frac{a_0 * p}{100}\right) * Rnd, \quad (2.13)$$

where a_0 is the original non-randomized variable and Rnd is a random number between 0 and 1. This results in $0.8a_0 < a \leq 1.2a_0$ for a 20% deviation. Thus, the locations of the centre points of the surface feature are randomized. The code then checks all points (x, y) on the surface such that $x_0 - 2a \leq x \leq x_0 + 2a$ and $y_0 - 2a \leq y \leq y_0 + 2a$ to ensure that the (x_0, y_0) are within the grid boundary. The points (x, y) are then assigned a height value according to Equation 2.12.

If the points are not empty, the code computes the value of Equation 2.12, compares

it with the value already in the array, and selects the larger value. The program then checks to see if the point (x_0, y_0) is a maximum or a minimum. A maximum indicates that the surface feature does exist around this point. This method is repeated until the grid is filled with paraboloidic surface features. An example of an elliptical paraboloid can be seen in Figure 2.9

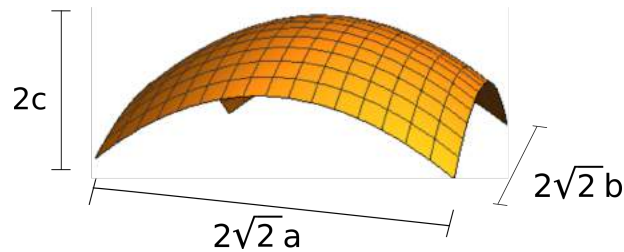


Figure 2.9: An example of an elliptical paraboloid. The parameters a and b control the curvature of the object, while c controls the vertical elongation.

Next, the program computes 10 surfaces based on the same initial conditions plus randomness, and calculates the averages of the statistical parameters. It then repeats this process for varying a , c , and z_0 , as determined by the start, end and step size fields in the GUI (Figure 2.8). Note that, to create round surface features, the parameters, a and b , were kept equal. Finally, the boundary is removed, the statistical parameters are calculated, the surface image, distribution and cross-sectional plots are displayed in the GUI, and the statistical data are written to file. An example of a corrugated surface can be seen in Figure 2.2b and examples of the cross-sectional plot and the distribution can be seen in Figure 2.10.

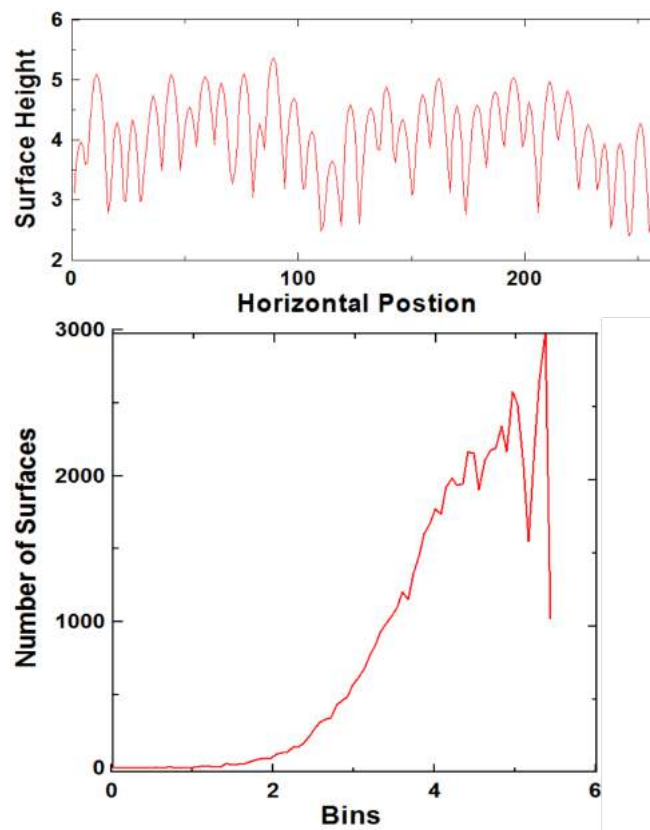


Figure 2.10: A sample of the cross-section (top) and the surface height distribution (bottom) outputs from the corrugated surfaces simulation.

Chapter 3

Results and Discussion

3.1 Corrugated Surfaces Results

For the corrugated surfaces simulations, we set $b = a$ and allowed a and c to vary from 10 to 70, and z_0 to vary from 0 to 20 all in steps of 2. The previously mentioned statistical parameters were computed for these surfaces 10 times and averaged to account for the randomness in the parameters for each surface. The grid size, g , was set to 8 and the resolution, G , to 256 for all surfaces. Figure 3.1 shows a comparison of a gold surface, imaged by atomic force microscopy (AFM), and a computer generated corrugated surface. Figure 3.1a was generated with $a = 60$, $c = 50$ and $z_0 = 16$. The vertical length scale is displayed in greyscale, with the highest features displayed as

white, and the lowest features displayed as black. The size of the surface shown in Figure 3.1b is 1000 nm \times 1000 nm, with surface features ranging from 0 – 19 nm in height. The surfaces appear visually similar to one another.

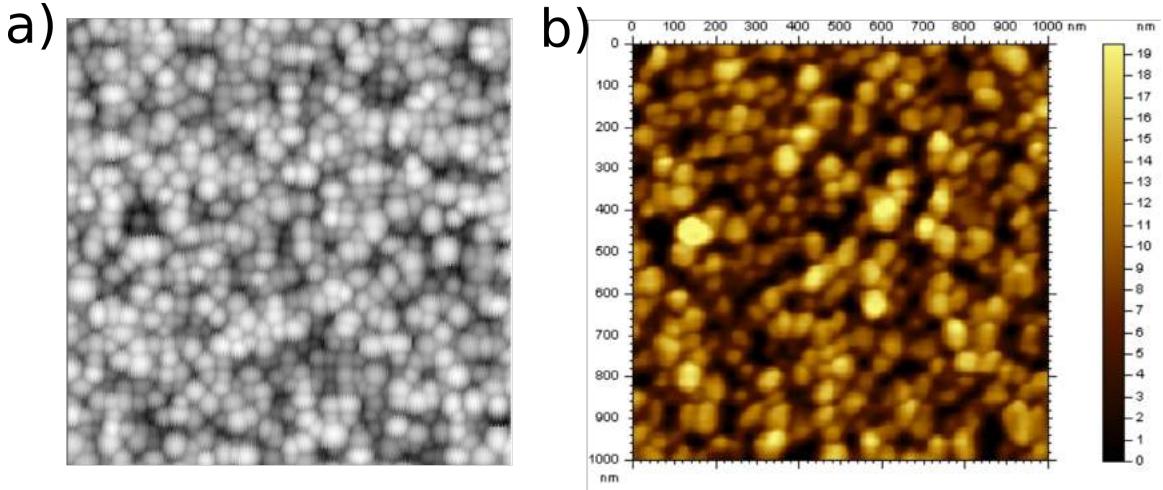


Figure 3.1: a) A computer-generated corrugated surface compared with a b) AFM image of a gold surface.

It is first useful to examine how the shape of an elliptic paraboloid changes with values of a and c . Figure 3.2 shows sample parabolas with various values of a and c . Note that larger values of a lead to wider parabolas, while larger values of c lead to narrower parabolas. It is also useful to examine how surfaces change with one parameter, while keeping the others constant. Figure 3.3 shows surfaces for different values of a and constant values of c and z_0 . All three surfaces are visually similar, however the maximum of height from the cross-sectional plot can be observed to

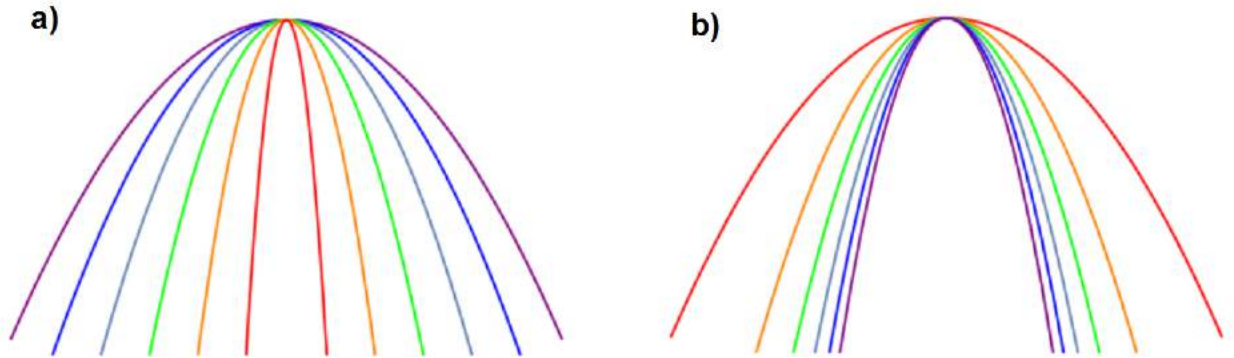


Figure 3.2: a) Parabolas with $c = 10$ and a ranging from $a = 10$ (red), $a = 22$ (orange), $a = 34$ (green), $a = 46$ (turquoise), $a = 58$ (blue), and $a = 70$ (violet). b) Parabolas with $a = 10$ and c ranging from $c = 10$ (red), $c = 22$ (orange), $c = 34$ (green), $c = 46$ (turquoise), $c = 58$ (blue), and $c = 70$ (violet).

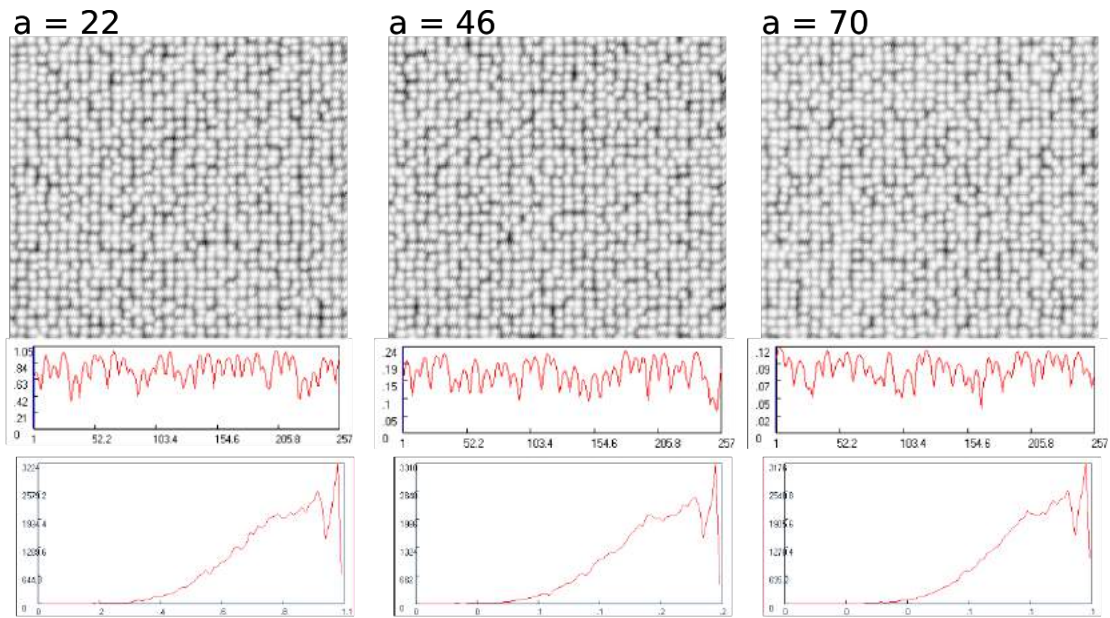


Figure 3.3: Examples of computer-generated corrugated surfaces with varying a , along with a cross-sectional plot, and the surface height distribution for each surface. Each surface has $c = 10$ and $z_0 = 0$.

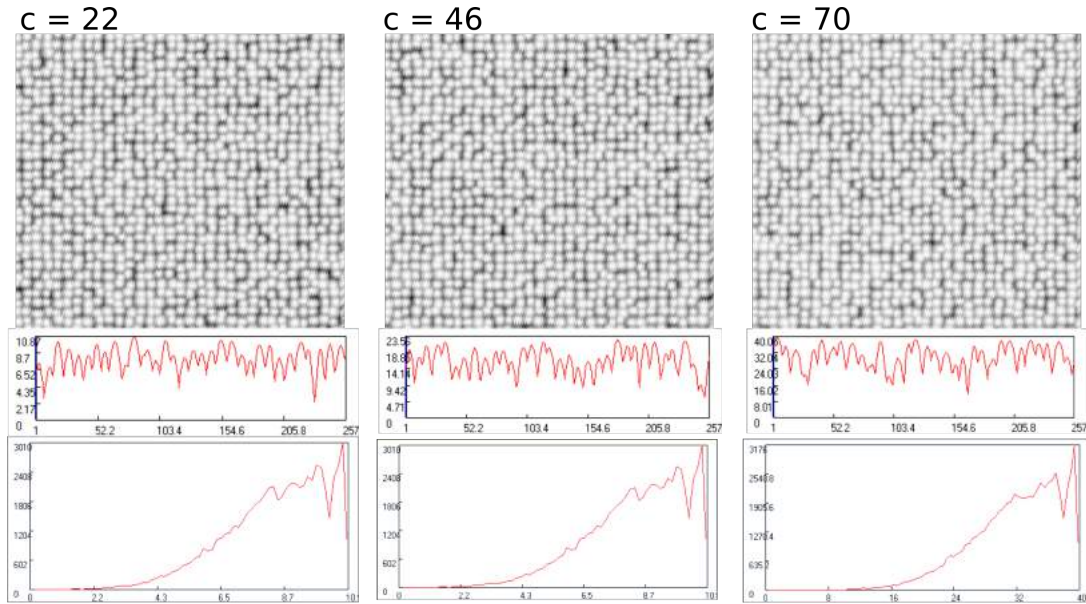


Figure 3.4: Examples of computer-generated corrugated surfaces with varying c , along with a cross-sectional plot, and the surface height distribution for each surface. Each surface has $a = 10$ and $z_0 = 0$.

decrease from 1.05 to 0.12 as a increases. This implies that as a increases, the height of surface features tend to decrease. The a parameter controls the in-plane elongation of each hemispherical paraboloid, so increasing a with c constant causes the feature to flatten, resulting in lower surface height. This also causes a decrease in the range of surface height, as shown in the cross-sectional plots, so the height of the features will tend to cluster near similar, smaller values, thus decreasing the variance across surface features.

Figure 3.4 shows surfaces with changing values of c and constant values of a and

z_0 . As with Figure 3.3, these surfaces are not significantly visually different, however the maximum surface height from the cross-sectional plot can be seen to increase from 10.87 to 40.06, with the range of bins in the distribution increasing accordingly. The c parameter controls the vertical elongation of a hemispherical paraboloid, and so increasing c with a constant causes the feature to stretch, which gives larger surface height.

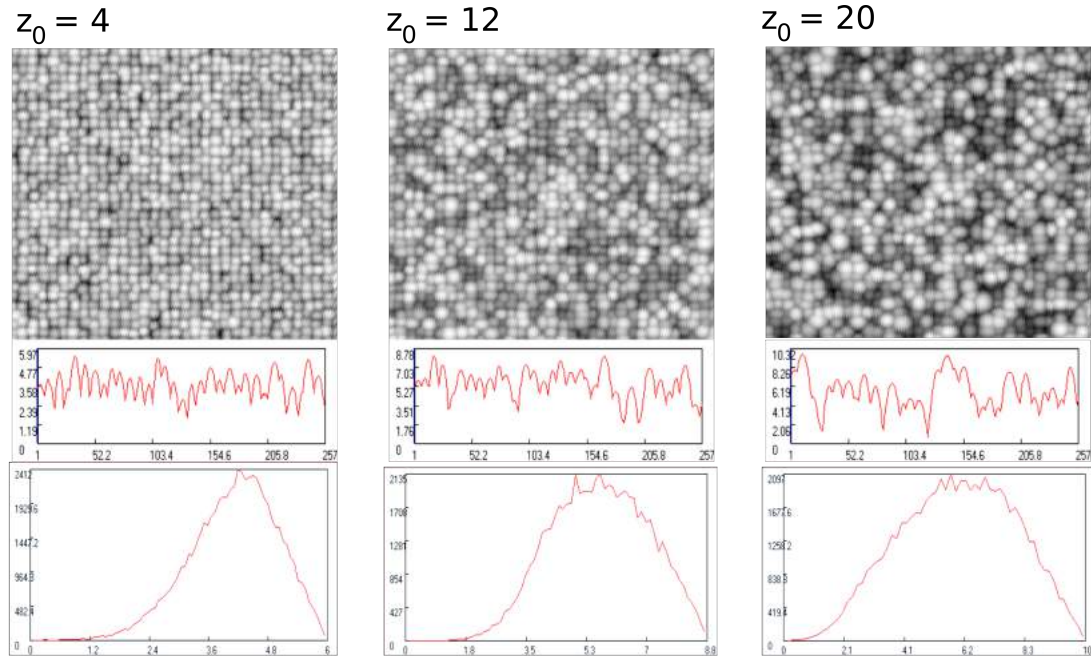


Figure 3.5: Examples of computer-generated corrugated surfaces with varying z_0 , along with a cross-sectional plot, and the surface height distribution for each surface. Each surface has $a = 10$ and $c = 10$.

Figure 3.5 shows surfaces with changing values of z_0 and constant values of a and c .

As z_0 increases, it is clear from the cross-sectional plot that the maximum surface

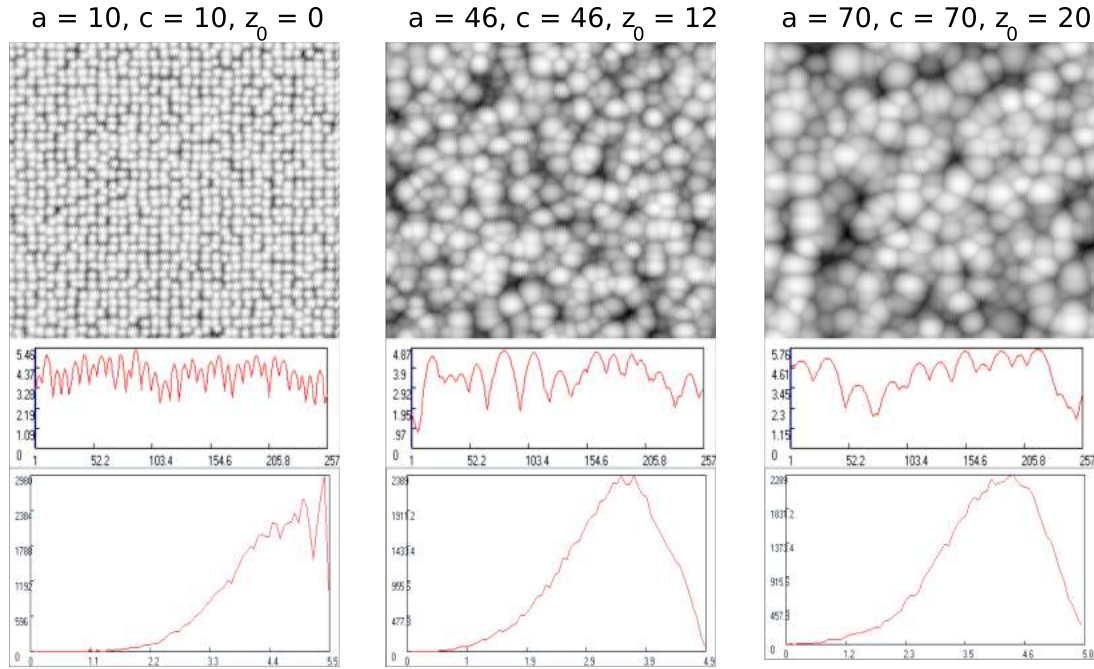


Figure 3.6: Examples of computer-generated corrugated surfaces with a , c , and z_0 all varying.

height increases from 5.97 to 10.32. Further, the variation in the surface height also increases slightly. These differences, although significant, are much less than the changes observed for varying c in Figure 3.4. This is because z_0 affects the waviness, whereas a and c affect the roughness (see Chapter 2 for discussion on waviness). The c parameter, therefore, has a much greater effect on the roughness parameters than z_0 . From the distribution plots, we can see a slight shift to the left as z_0 increases, as well as a widening of the peak of the distribution; this is caused by the increasing variation in surface height, and is indicative of small changes in the skewness and

kurtosis.

Figure 3.6 shows sample surfaces in which all parameters are changing. From the cross-sectional plot, we see that the maximum height stays relatively constant across the surfaces. This is due to the fact that increasing c increases the RMS roughness, while increasing a decreases the RMS roughness, while z_0 only affects the waviness. Thus the effects largely offset, and only a slight increase in surface height is observed. We note as well that the width of the peak of the distribution increases only slightly; this is due to the aforementioned offsetting effect.

With these behaviours in mind, we now examine the statistical parameters. Due to the fact that the RMS roughness has units of length, this parameter is affected by the length scale of the surface height of the surfaces under study, which may be arbitrary. To account for this, it is important to plot the statistical parameters against non-dimensionalized a and c parameters. To create a non-dimensionalized a value, we introduce the nearest neighbour distance, NND , as the average horizontal distance between two adjacent particles on a surface, and calculate it using the following equation,

$$NND = \frac{\sqrt{N}}{g} \quad (3.1)$$

where N is the number of particles on the surface, and so \sqrt{N} is approximately the number of particles along one side of the surface, and g is the grid size. A natural choice of non-dimensionalized parameter is thus $a^* = \frac{a}{NND}$, which is a measure of the horizontal size of the particles relative to the surface size. Figure 3.7a shows a corrugated surface cross-section with no randomness, while Figure 3.7b shows a zoom-in of the same surface. Both a and NND appear larger in Figure 3.7b, however their ratio will be the same for both surfaces, accurately representing the fact that these two surfaces are identical.

In Figure 3.8a, the roughness parameters are plotted against a^* . Note that curves of different colours represent different statistical parameters, while curves using different shaped markers represent different values of c . Neither the skewness nor kurtosis change with a^* at any value of c , while the remaining parameters decrease with a^* at all values of c . This behaviour appears exponentially decreasing for high values of c . Similar behaviour is observed in Figure 3.8b, in which the markers represent different values of z_0 , for all parameters, with the exception of the surface area ratio, which remains largely constant for all values of a and z_0 . This is due to the fact that this data was taken at $c = 10$, which is consistent with the $c = 10$ surface area ratio curve in Figure 3.8a. Additionally, the range of a^* for each of the 5 curves corresponding to $z_0 = 0$ is much smaller than for other z_0 values. This is due to the fact that surfaces

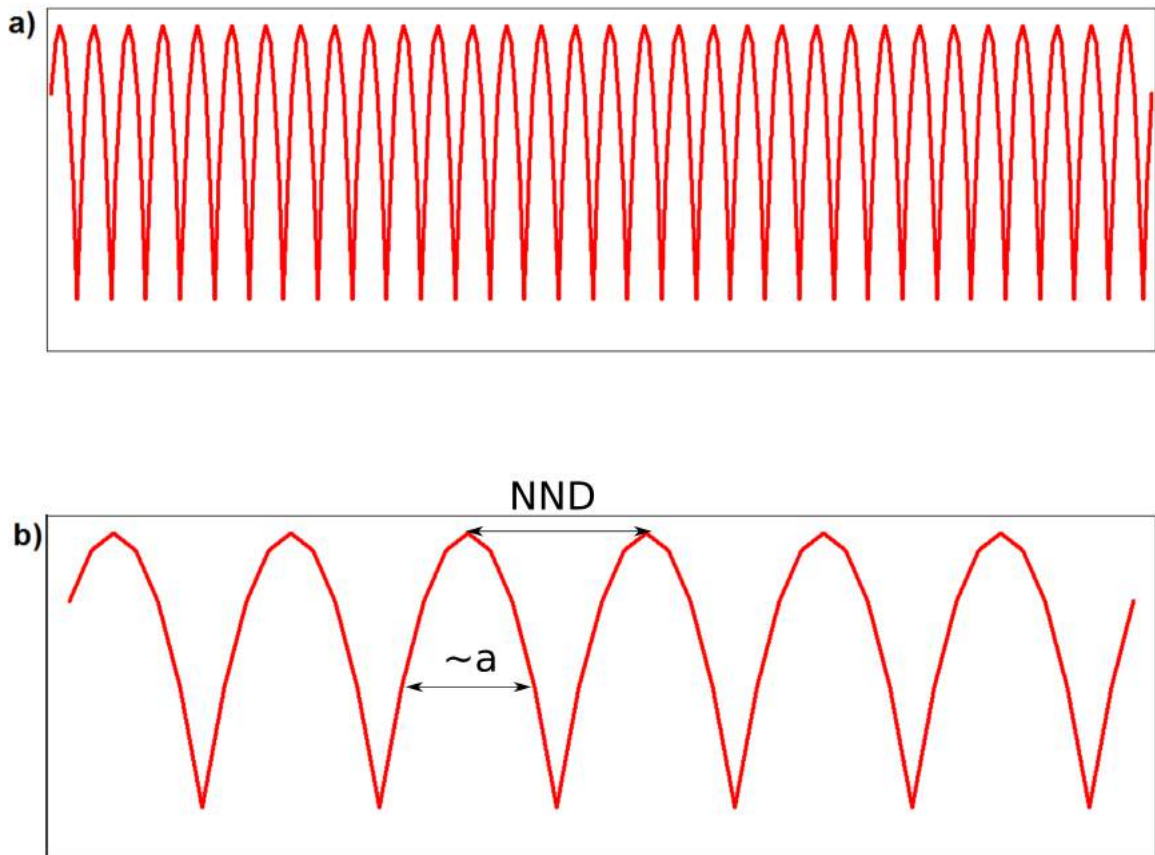


Figure 3.7: a) A periodic corrugated surface without randomness. b) A zoom-in of a). Both a and NND are shown, and appear larger than they would in a).

with $z_0 = 0$ have approximately the same number of particles for all a , whereas for surfaces with other z_0 values, the number of particles tends to decrease with increasing a , giving a larger range of a^* values. The similar number of particles for surfaces with $z_0 = 0$ can be explained by considering that the particles of such a surface will have little height variation compared with surfaces with higher z_0 values. Thus, the tails of the elliptic paraboloids that make up the surface will have less space to spread

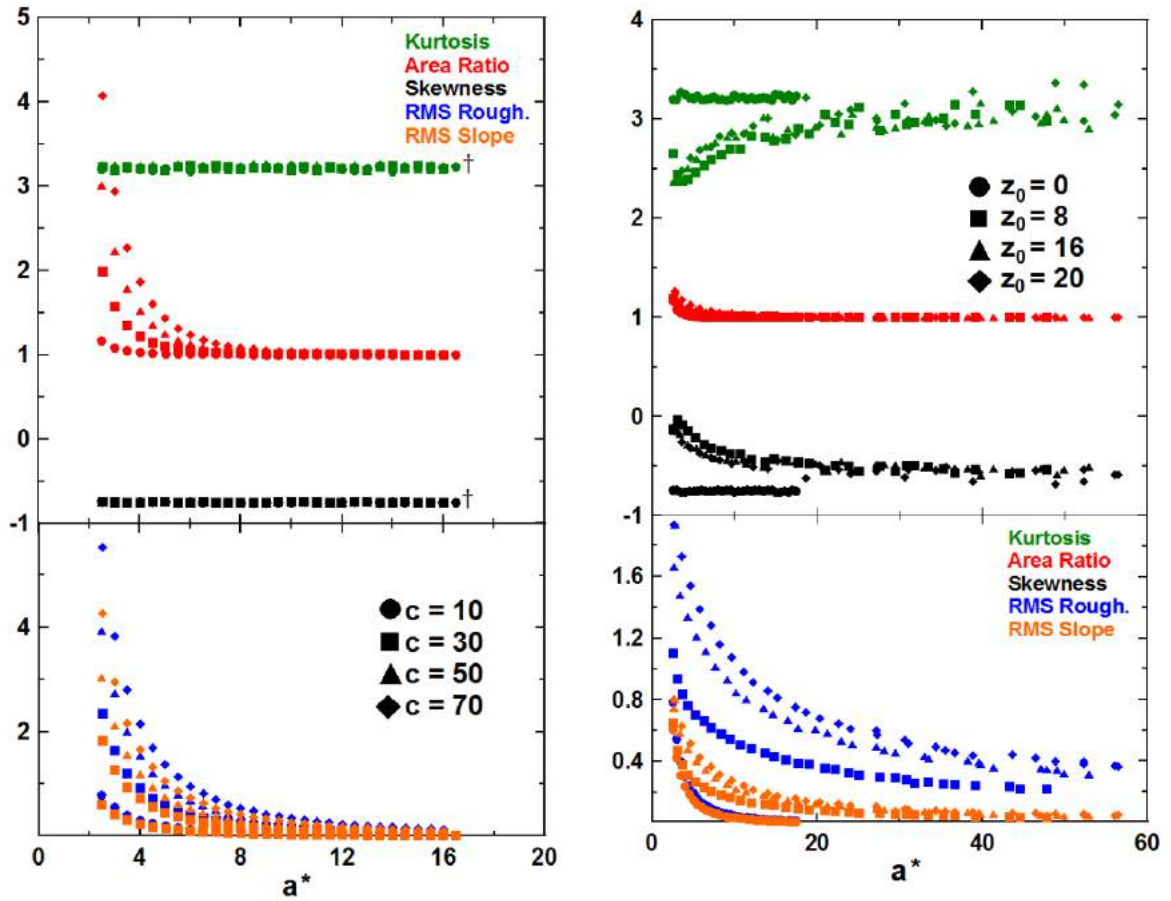


Figure 3.8: a) Statistical parameters vs. a^* . Circles represent $c = 10$, squares represent $c = 30$, triangles represent $c = 50$, and diamonds represent $c = 70$. All data in this plot has $z_0 = 0$. b) Statistical parameters vs. a^* . Circles represent $z_0 = 0$, squares represent $z_0 = 8$, triangles represent $z_0 = 16$, and diamonds represent $z_0 = 20$. All data in this plot has $c = 10$. † Several sets of data are overlapping in this plot.

out, and will cover a smaller horizontal distance, leading to more horizontal space on the surface for additional particles.

A similar parameter $c^* = \frac{c}{NND}$ can be also be computed. This parameter gives a measure of the vertical size of the particles compared to the surface size, and has no

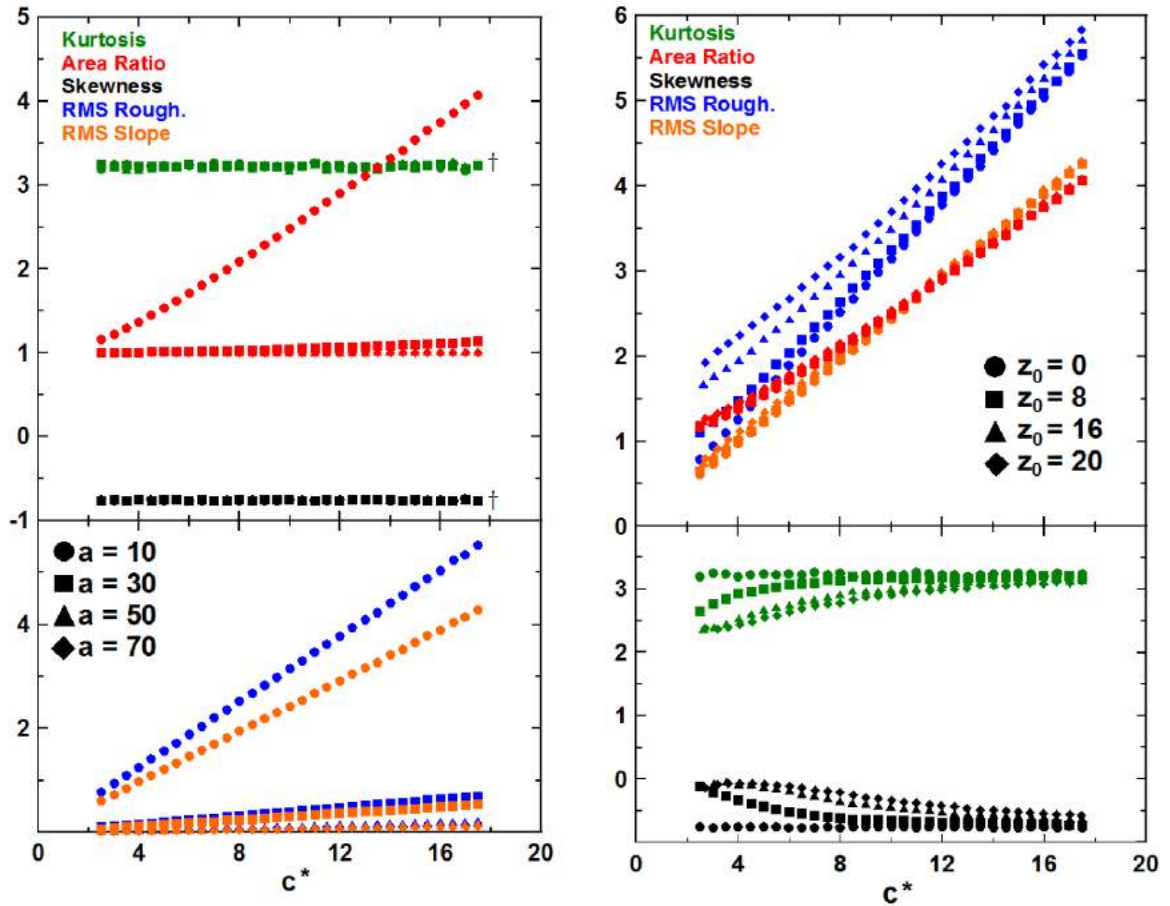


Figure 3.9: a) Statistical parameters vs. c^* . Circles represent $a = 10$, squares represent $a = 30$, triangles represent $a = 50$, and diamonds represent $a = 70$. All data in this plot has $z_0 = 0$. b) Statistical parameters vs. c^* . Circles represent $z_0 = 0$, squares represent $z_0 = 8$, triangles represent $z_0 = 16$, and diamonds represent $z_0 = 20$. All data in this plot has $a = 10$. † Several sets of data are overlapping in this plot.

dimensions. Figure 3.9a shows the RMS roughness, RMS slope, surface area ratio, skewness and kurtosis against c^* with different shaped markers representing different values of a . We observe that the skewness and kurtosis remain constant for all values of c^* , and over the range of a values, while the RMS slope, RMS roughness, and

surface area ratio are largely constant for high values of a , but change linearly with c^* at low values of a . In Figure 3.9b, the different shaped markers now represent different values of z_0 . Skewness and kurtosis change only slightly with respect to c^* , at all values of z_0 . The RMS roughness, RMS slope, and surface area ratio increase linearly with c^* and are shifted to larger values for increasing z_0 .

Figure 3.10a shows the statistical parameters against z_0 , with markers representing different values of c . We observe, again, the slight increase in RMS roughness, RMS slope, and surface area ratio with z_0 , and the large increase of these parameters with c . Skewness and kurtosis are largely constant with increasing z_0 for all values of c . In Figure 3.10b, the markers represent different values of a . At all values of a , the skewness, kurtosis, RMS slope, and surface area ratio are constant with increasing z_0 , while the RMS roughness increases with z_0 at low values of a . The RMS slope is shifted vertically upward for lower values of a .

For the purposes of surface characterization, it is useful to examine the shape of the S_{ku} vs. S_{sk} curve. Figure 3.11 shows a plot of kurtosis against skewness with the RMS roughness represented by the colour of the plot points. From this plot, the ranges of skewness and kurtosis values are small, with skewness values from -0.77 to -0.03 and kurtosis values from 2.35 to 3.36 .

The plot of kurtosis vs. skewness is doubly-valued, implying that there are two po-

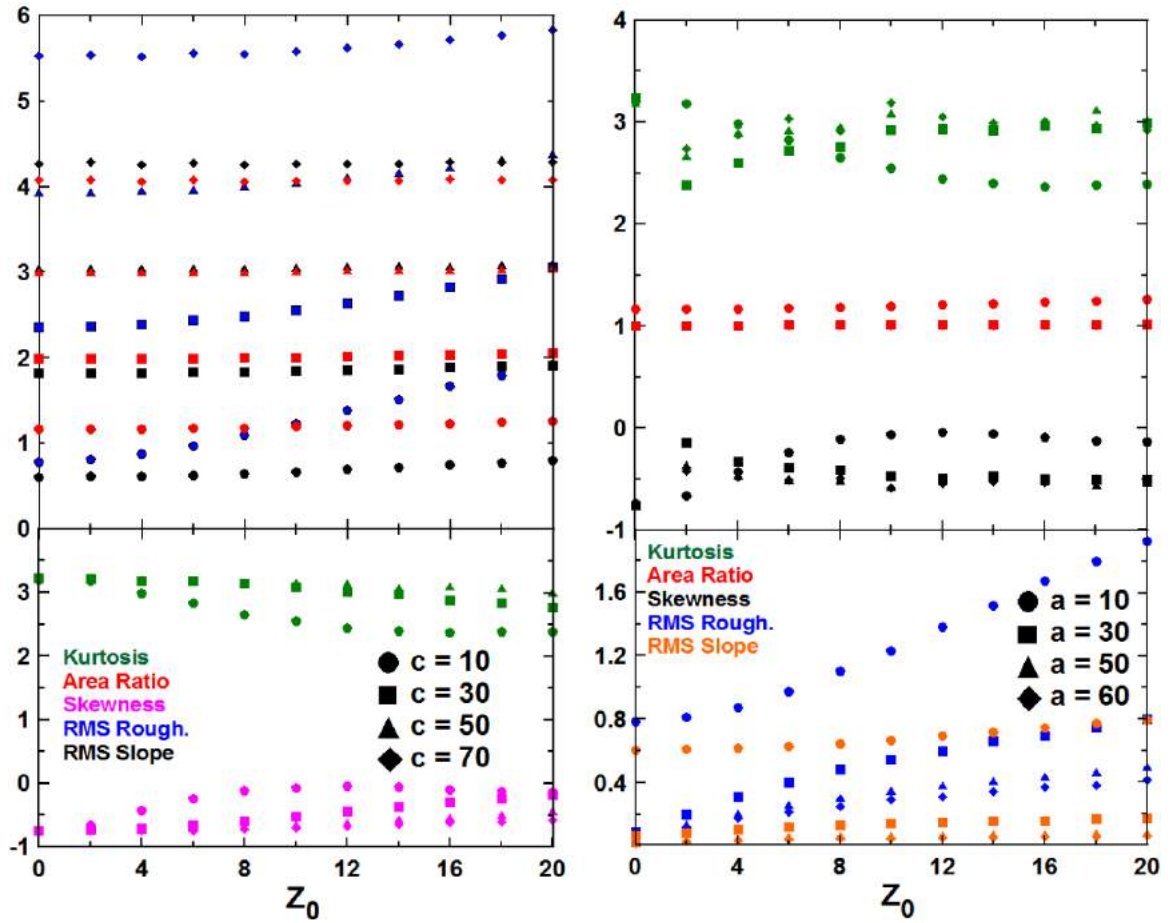


Figure 3.10: a) Statistical parameters vs. z_0 . Circles represent $c = 10$, squares represent $c = 30$, triangles represent $c = 50$, and diamonds represent $c = 70$. All data in this plot has $a = 10$. b) Statistical parameters vs z_0 . Circles represent $a = 10$, squares represent $a = 30$, triangles represent $a = 50$, and diamonds represent $a = 60$. All data in this plot has $c = 10$.

tential values of kurtosis which correspond to a particular value of skewness. Further, the RMS roughness can be significantly different for surfaces with similar skewness and kurtosis, as evidenced by the close proximity of red and blue points, and there

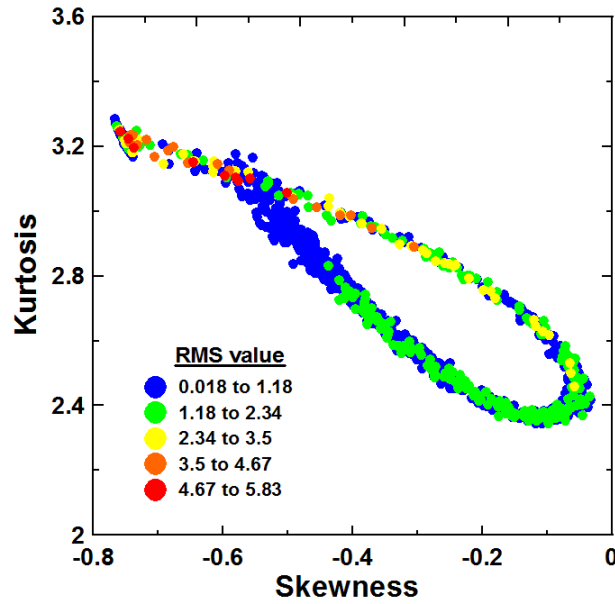


Figure 3.11: Kurtosis vs. skewness with RMS roughness represented with colour. The RMS roughness ranges from 0.018 (blue) to 5.83 (red).

is a large overlap between many of the colours, further implying that many different surfaces can have similar skewness and kurtosis. Due to the monotonicity of the RMS roughness, this implies that the skewness and kurtosis cannot be related to the roughness of the surface. This fact, combined with the lack of significant change in skewness and kurtosis over the range of a , c , and z_0 values provides evidence to conclude that the skewness and kurtosis are insensitive to surface morphology and are thus not applicable to surface characterization or roughness measurement of corrugated surfaces.

3.2 Abraded Surfaces Results

For abraded surfaces simulations, the number of scratches per surface was varied from 4 to 300. The scratch radius distribution was also varied, using different proportions of coarse, medium, fine, and superfine scratches. The maximum scratch radius was set to 6 for all simulations unless otherwise stated. Figure 3.12 shows a comparison of a simulated abraded surface and an actual abraded surface. The simulated surface was generated with 200 scratches, and appears similar to the image of a scratched surface, prepared by Dr. Marko Sedlaček. [10].

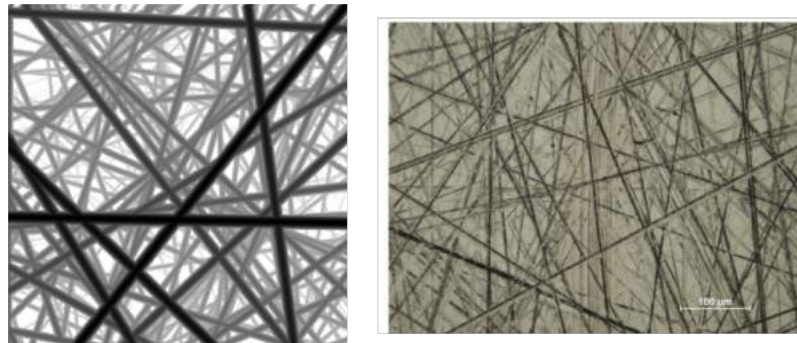


Figure 3.12: Left: A sample simulated abraded surface with 200 scratches. Right: A scratched surface displayed with permission from Dr. Marko Sedlaček.

Statistical parameters were calculated for sets of abraded surfaces with different scratch radius distributions. The a) sides of Figures 3.13- 3.17 show the results of these simulations. The shapes of the curves for each parameter are similar for different distributions, with only minor differences. Distributions with more fine and superfine

scratches tend to have a larger range of kurtosis and skewness, while distributions with more coarse scratches have smaller ranges. This is due to the fact that surfaces with smaller percent coverage of scratches have higher skewness and kurtosis, and a superfine scratch will cover less of a portion of the surface than a coarse scratch. Thus, surfaces composed mainly of smaller scratches will have higher skewness and kurtosis for lower percent coverage than surfaces with larger scratches, resulting in a larger overall range of skewness and kurtosis.

As percent coverage approaches 100%, for surfaces composed mostly of fine and superfine scratches, the skewness and kurtosis tend towards their Gaussian values, while for surfaces composed mostly of medium and coarse scratches, the skewness and kurtosis begin to increase after reaching their Gaussian values. For all distributions, the change in the RMS slope, and surface area ratio is relatively small. The RMS roughness increases along the curve for all distributions and has a peak at Gaussian skewness and kurtosis values; this can also be seen from the b) sides of Figures 3.13 - 3.17. Thus, the roughest abraded surfaces have Gaussian skewness and kurtosis values.

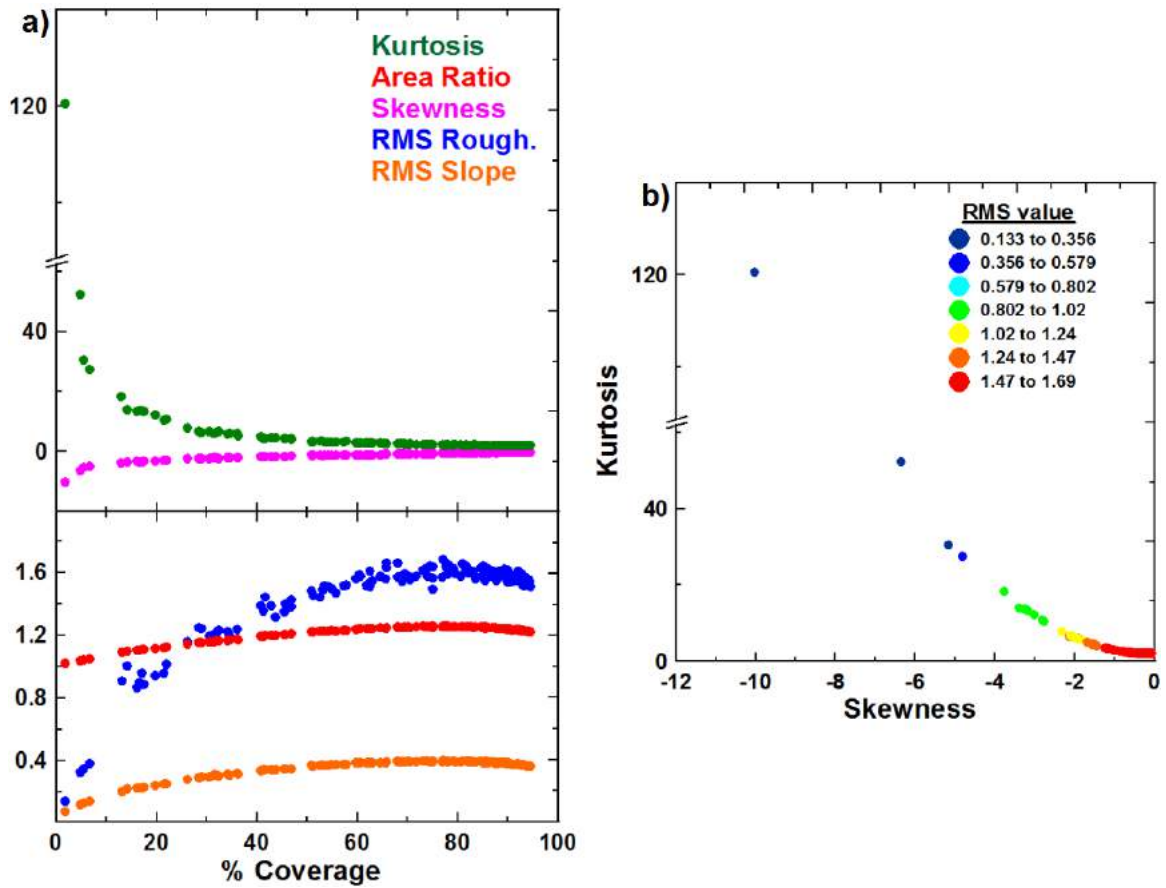


Figure 3.13: a) Statistical parameters for surfaces with a scratch depth distribution of 5% coarse, 5% medium, 10% fine and 80% superfine scratches. b) Kurtosis vs. skewness for this distribution.

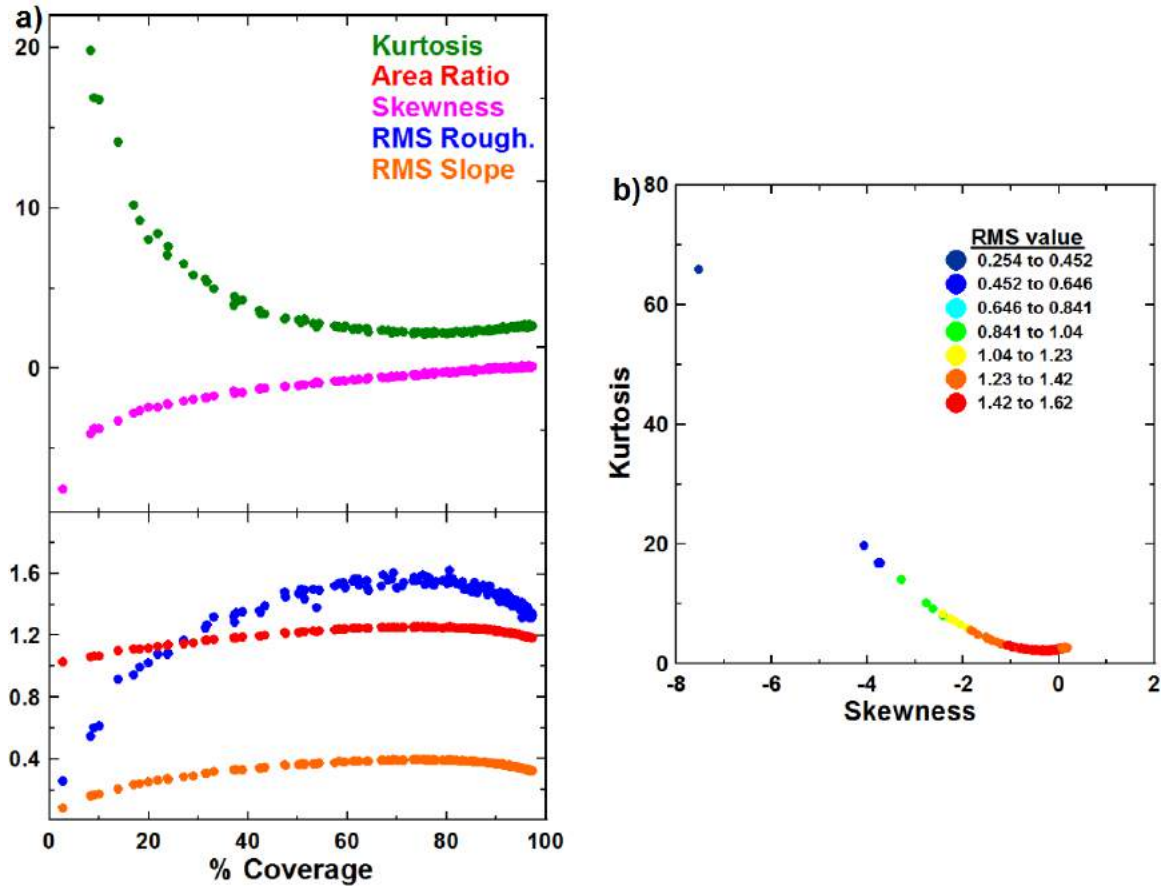


Figure 3.14: a) Statistical parameters with a scratch depth distribution of 5% coarse, 10% medium, 25% fine and 60% superfine scratches. b) Kurtosis vs. skewness for this distribution.

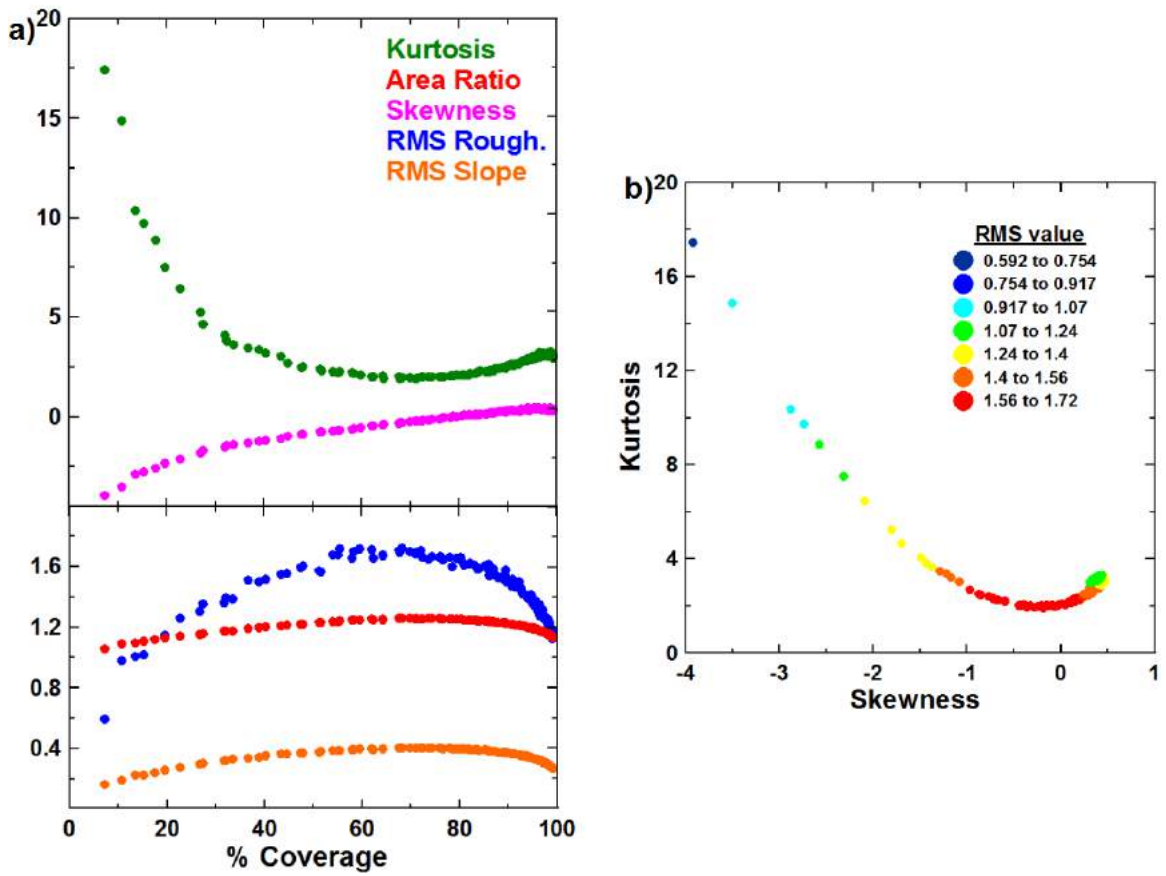


Figure 3.15: a) Statistical parameters with a scratch depth distribution of 10% coarse, 20% medium, 40% fine and 30% superfine scratches. b) Kurtosis vs. skewness for this distribution.

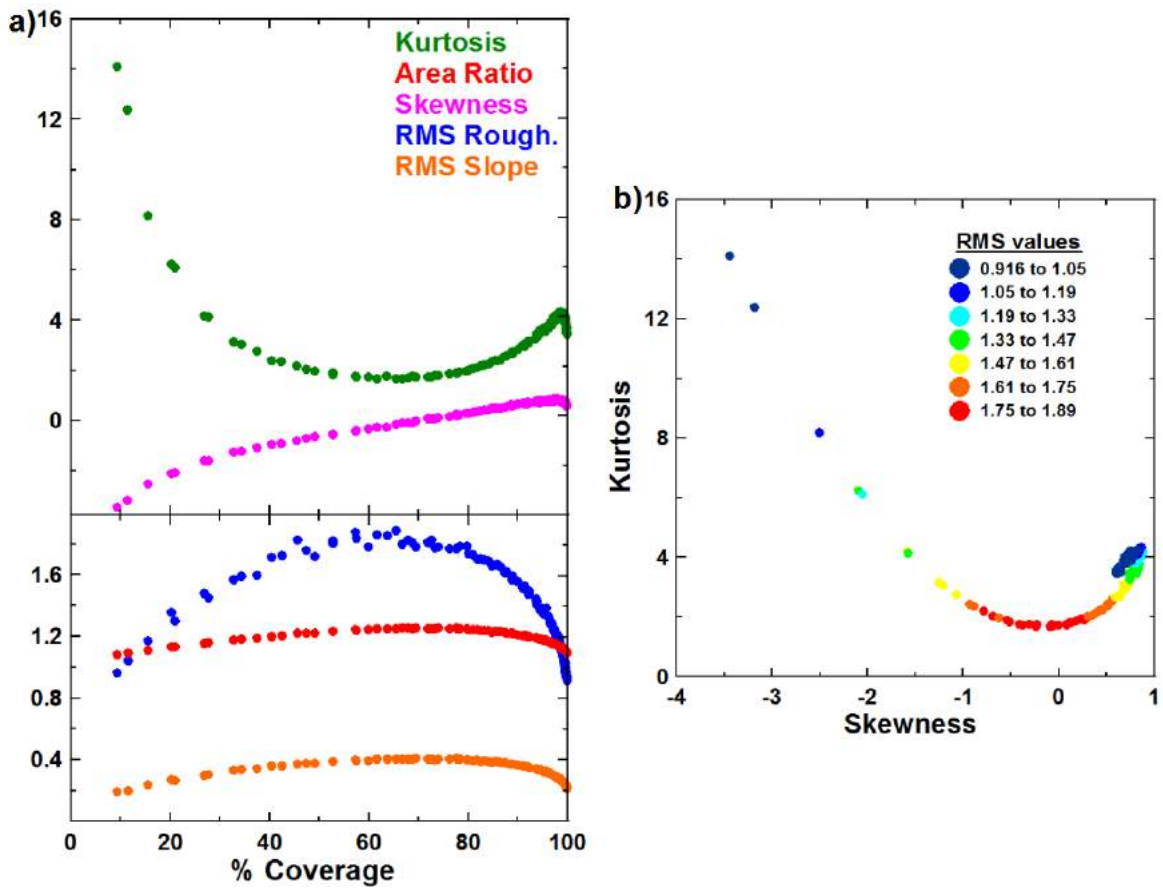


Figure 3.16: a) Statistical parameters with a scratch depth distribution of 20% coarse, 40% medium, 30% fine and 10% superfine scratches. b) Kurtosis vs. skewness for this distribution.

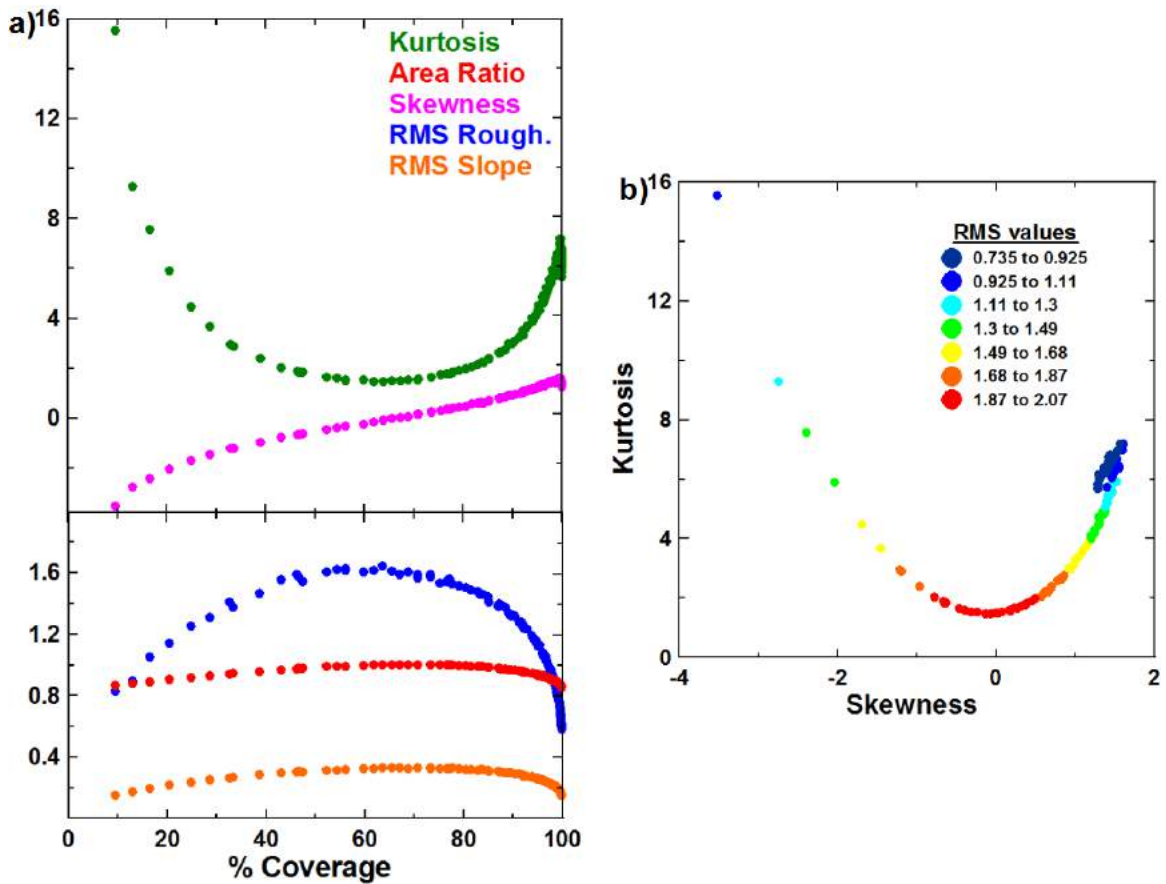


Figure 3.17: a) Statistical parameters with a scratch depth distribution of 40% coarse, 30% medium, 20% fine and 10% superfine scratches. b) Kurtosis vs. skewness for this distribution.

The kurtosis vs. skewness curves are single-valued for scratch radius distributions mainly composed of smaller scratches, however this is not the case for distributions composed of larger scratches. For distributions with larger scratches, the kurtosis begins to increase with skewness beyond the Gaussian skewness and kurtosis values. Figure 3.18a shows the cross-section of an abraded surface composed mainly of

smaller scratches, and is compared with Figure 3.18b, which shows an abraded surface composed mainly of larger scratches. It is clear that many of the scratches shown in the plot in Figure 3.18a are small enough to extend to their lowest depth, and back up to the $z = 0$ line. In contrast, the scratches in Figure 3.18b are prevented from extending back up to $z = 0$ due to overlap with other scratches. This results in a lower surface maximum of approximately $z = -2$ in Figure 3.18b in contrast to a maximum of $z = 0$ in Figure 3.18a.

In contrast to the results from the corrugated surfaces simulations, the RMS roughness is a simple function along the kurtosis vs. skewness curves. For surfaces composed of mainly smaller scratches, the simple, single-valued function could be useful in determining any of the skewness, kurtosis, or RMS roughness, given any two of the parameters. However, due to the multi-valued nature of surfaces composed of larger scratches, the relationship between the skewness, kurtosis, and RMS roughness is more complex than for surfaces composed of smaller scratches. Thus, our model breaks down for surfaces composed of larger scratches as the percent coverage approaches 100%.

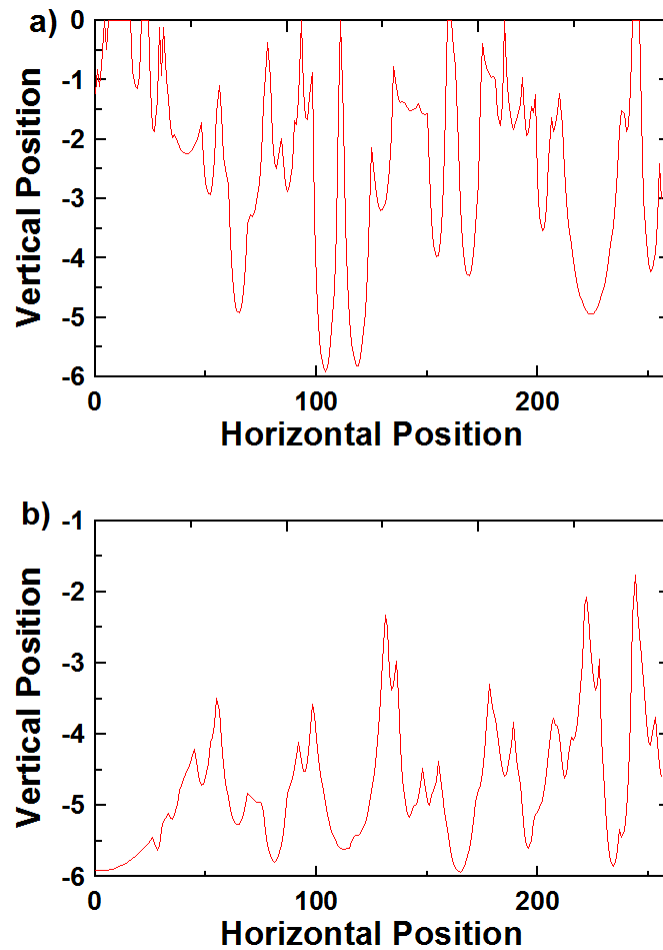


Figure 3.18: A comparison of a) a cross-section of an abraded surface composed of 200 scratches distributed with a majority of smaller scratches, and b) a cross-section of an abraded surface composed of 200 scratches distributed with a majority of larger scratches. Note that the maximum scratch height in a) is approximately 0, while the maximum scratch height in b) is approximately -2 .

3.3 Discussion

From the corrugated surfaces simulations, it was observed that, for some surfaces, the RMS roughness changed significantly, while the skewness and kurtosis remained largely constant. The significant change in the RMS roughness for corrugated surfaces is due to the effect of only a small number of surfaces which have the lowest a^* values, the highest c^* , and the highest z_0 values sampled. These surfaces have the highest RMS values of any surfaces generated in these simulations. The small a^* values imply that a greater number of hemispherical grains is placed on the surface, due to the low values of a and high values of N , and the high c^* and z_0 values both vertically elongate and raise each grain respectively. These factors have the effect of increasing the RMS roughness to values approximately 5 times higher than the RMS roughness values of most other surfaces in these simulations. However, these surfaces appear ordered (as in Figure 3.4) compared to, for example, surfaces with the highest a^* values as well as the highest c^* and z_0 values (Figure 3.6), which have RMS roughness values 5 times smaller than for surfaces with the lowest a^* , c^* , and z_0 values. This ordering of surface features is not observed when considering surfaces prepared by thermal or sputter deposition, as in Figure 3.1. For a surface prepared by thermal or sputter deposition, each individual surface feature will have a different degree of horizontal

elongation, leading to a lower surface feature density than if all features had low a values, and so the RMS roughness may not have as large a range for these surfaces. Thus, the RMS roughness will change significantly only for a small number of surfaces which have the correct combination of a , c , and z_0 , and may not undergo significant changes for other surfaces.

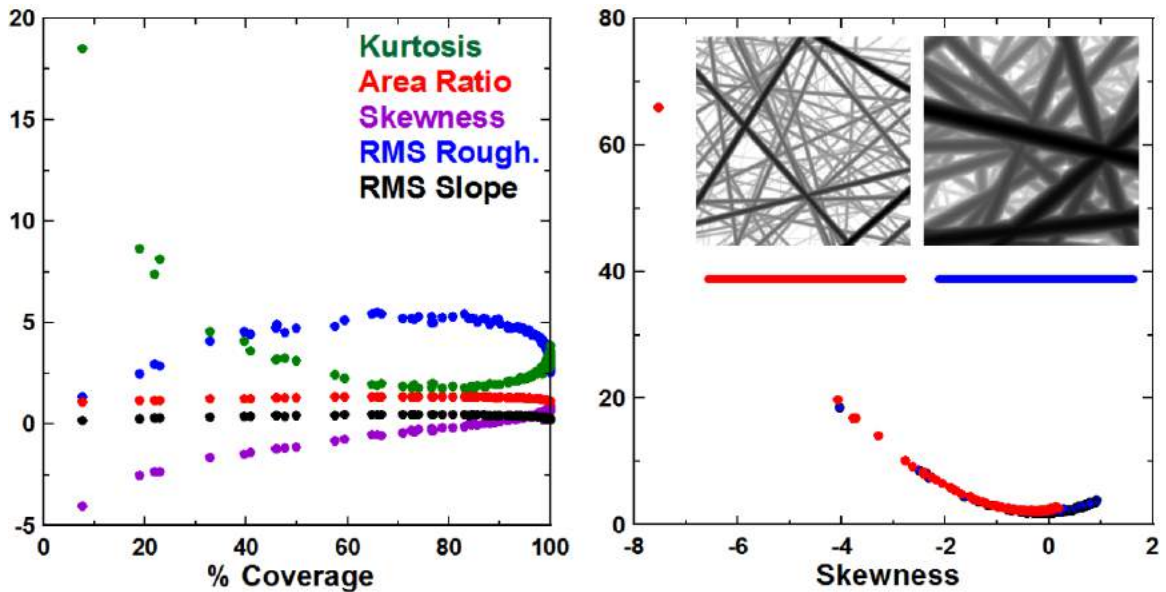


Figure 3.19: a) Statistical parameters for surfaces with a scratch depth distribution of 5% coarse, 10% medium, 25% fine and 60% superfine scratches, with a maximum radius of 18. Note the increase in the range of RMS roughness as compared with Figure 3.14. b) The kurtosis vs. skewness curve for the same distribution as a), for simulations conducted with maximum radii of 6 (red) and 18 (blue).

For the abraded surface simulations, the RMS roughness showed less significant change than the skewness and kurtosis, which changed significantly. The small change in RMS roughness for abraded surfaces is due to the fact that abraded surfaces are

composed of features which do not vary significantly from one to another. A scratch with a radius of 1.5, a superfine scratch, in a resolution of 256 occupies 0.6% of the surface size, whereas a scratch with a radius of 6, a coarse scratch, occupies 2.3% of the surface size, giving a range of 1.7%. If the maximum radius were increased, however, then the scratch radius range would increase, and thus we would expect to see an increase in the range of the RMS roughness. Figure 3.19a shows that this is indeed the case; simulations with the same scratch radius distribution, but a larger maximum scratch radius will increase the range of the RMS roughness. Note that, from Figure 3.19b, the kurtosis vs. skewness curve is nearly identical to that of Figure 3.14b. Surfaces with large, deep scratches as in Figure 3.19 appear to be a zoomed in version of the scratch pattern shown in Figure 3.12. From Figure 3.12 and from the literature, [10], scratches in physically realistic abraded surfaces show little variation due to how the surfaces were abraded. Thus, the applicability of the RMS roughness in characterizing the surface roughness is limited to surfaces composed of many types of scratches.

Figure 3.19b shows that the skewness and kurtosis of abraded surfaces change only slightly with scratch distribution, with surfaces composed of larger scratches showing a slight increase in kurtosis with skewness beyond Gaussian skewness and kurtosis values. This is also seen by plotting the kurtosis vs. skewness curves for all

distributions sampled on the same set of axes, as in Figure 3.20. They are, however, affected by the degree to which the surface is covered by these features.

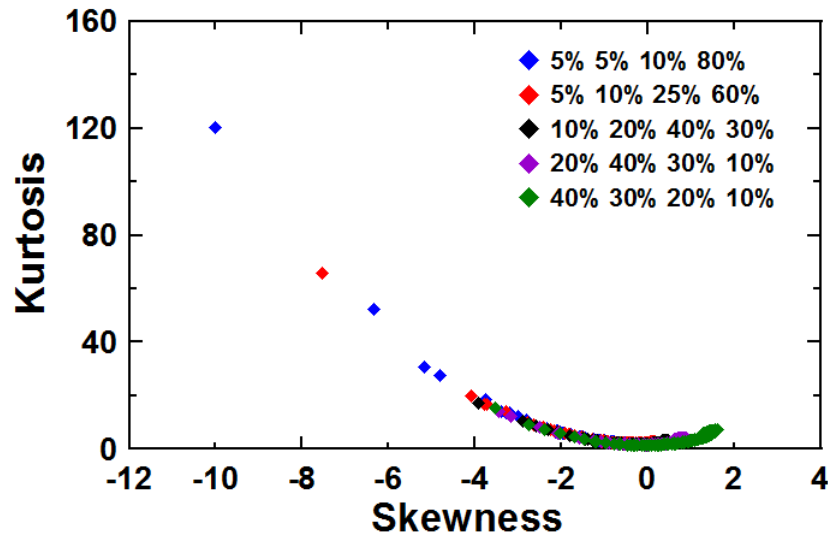


Figure 3.20: Kurtosis vs. skewness curves for all distributions sampled. Note that all distributions fall on a single, universal curve.

Corrugated surfaces can be thought of as always having 100% surface coverage, and thus will always have skewness and kurtosis values near the Gaussian values. Abrasions on a surface, however, intrinsically leave large portions of a surface unaltered. Unaltered surfaces have high kurtosis and low skewness, as seen most prominently in Figure 3.13 and as the percent coverage increases toward 100%, the skewness and kurtosis head toward their Gaussian values. This results in the large change observed in the skewness and kurtosis for abraded surfaces over the range of percent coverage, while, for corrugated surfaces, the skewness and kurtosis remain largely constant near

their Gaussian values. This can be explained by considering that, at high percent coverage, cross-sectional plots of abraded surfaces resemble inverted cross-sectional plots of corrugated surfaces, as shown in Figure 3.21. Thus, abraded surfaces, once completely covered in scratches, give similar roughness statistics as a corrugated surface.

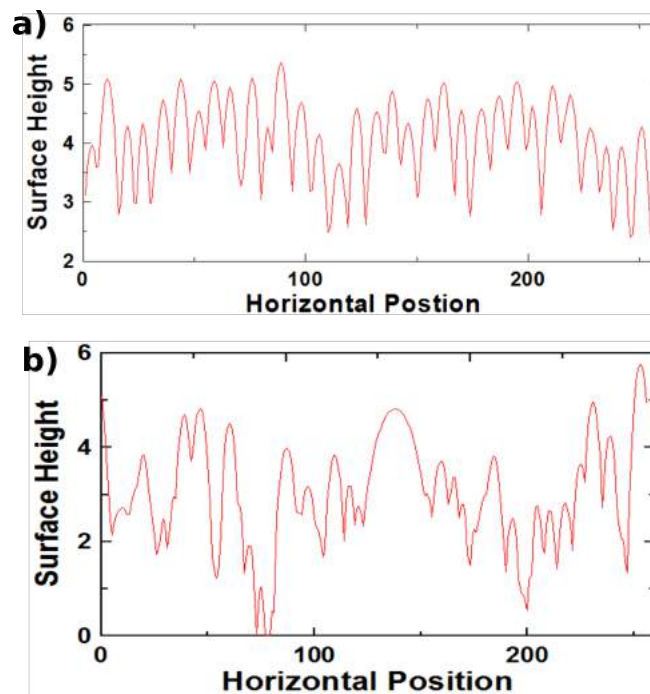


Figure 3.21: A comparison of a) the cross-sectional plot of a corrugated surface, and b) the inverted cross-sectional plot of an abraded surface composed of 300 scratches.

Chapter 4

Conclusions

In this work, two programs were written to simulate two types of surfaces: corrugated surfaces composed of hemispherical grains, and abraded surfaces composed of half-cylindrical scratches. Surface parameters, such as the a , c , and z_0 values for corrugated surfaces, and scratch radius, distribution, and surface coverage for abraded surfaces were varied to generate a large number of surfaces of both types. Statistical parameters including the RMS roughness, RMS slope, surface area ratio, skewness and kurtosis were then calculated for each surface. The objective of this study was to determine if the skewness and kurtosis could be related to the RMS roughness, and thus the surface roughness, for the purposes of surface characterization and roughness quantification.

For corrugated surfaces, it was observed that the skewness and kurtosis did not vary significantly for any of the non-dimensionalized parameters a^* and c^* , or for z_0 , while the RMS roughness increased slightly with z_0 and significantly with c^* at the lowest values of a^* . The lack of change in the skewness and kurtosis is due to the fact that unaltered surfaces, such as abraded surfaces with few scratches, can have kurtosis values as high as 120 (compared with the Gaussian value of $S_{ku} = 3$), and skewness values as low as -10 (compared with the Gaussian value of $S_{sk} = 0$). Corrugated surfaces are, by definition, completely covered by their surface features, resulting in skewness and kurtosis values that change little, and are approximately at their Gaussian values. The large change in the RMS roughness is a result of surfaces with the lowest a^* values and the highest c^* and z_0 values. The lowest a^* values result in surfaces with many particles, each with small horizontal elongation, while the highest c^* and z_0 values result in the highest and tallest surface features. This combination results in large RMS roughness values of approximately 5, which contrasts with other surfaces, which tend to have RMS roughness values up to 5 times smaller. The RMS slope and surface area ratio tend to follow the same behaviour as the RMS roughness as expected. In addition to having small ranges, a plot of kurtosis vs. skewness shows that there are two kurtosis values which correspond to a single skewness value. Further, the RMS roughness changes monotonically along

the plot, resulting in surfaces with the same skewness and kurtosis having entirely different values of RMS roughness. This indicates that the RMS roughness, skewness, and kurtosis cannot be related, which implies that the skewness and kurtosis are not applicable to surface characterization of corrugated surfaces.

For abraded surfaces, it was observed that the skewness and kurtosis did change significantly with percent surface coverage. Surfaces created from distributions composed mainly of larger scratches were found to have smaller ranges of skewness and kurtosis than surfaces created from distributions composed mainly of smaller scratches. Neither the skewness nor the kurtosis changed significantly with a changing range of scratch depths. For surfaces composed of mainly smaller scratches, the skewness and kurtosis approached their Gaussian values as the surface coverage increased to 100%. For surfaces composed of mainly larger scratches, the kurtosis began to increase with skewness beyond their Gaussian values. In contrast, corrugated surfaces, which can be thought of as being constantly at 100% coverage, always remain near their Gaussian values. This could be due to the fact that, as the percent coverage of an abraded surface increases to 100%, the surface begins to resemble an inverted corrugated surface, resulting in the roughness parameters for both being approximately equal. Changing the distribution of scratch radii affected the range of the skewness and kurtosis, but not the shape of the kurtosis vs. percent coverage and skewness vs.

percent coverage curves themselves. In fact, when kurtosis vs. skewness is plotted for all distributions, and overlaid on top of one another, all curves fall along a single, universal curve. This implies that the RMS roughness, skewness, and kurtosis are, in fact, related, and are entirely determined by the degree of surface coverage by the scratches, with the roughest surfaces occurring for Gaussian skewness and kurtosis values, at approximately 70% coverage. This relationship implies that it is possible to use the skewness and kurtosis, in conjunction with the RMS roughness, for surface characterization and roughness measurement. The RMS roughness, RMS slope, and surface area ratio did not change significantly with surface coverage, however the range of RMS roughness values did increase with increasing scratch radius range. Surfaces generated with a high maximum scratch radius showed a large increase in the range of RMS roughness values, while leaving the skewness and kurtosis unaffected. This is due to the fact that, for low maximum scratch radii, the range of radius is small compared to the size of the surface, resulting in only small variation between different scratches on a surface, and smaller RMS roughness values. Increasing this maximum radius allows for more variation, resulting in larger RMS roughness values, while maintaining the relation between skewness, kurtosis, and percent coverage.

4.1 Future Work

Although this is a terminal project for our group, some future work is possible. Experimental verification, by creating corrugated and abraded surfaces and measuring the roughness parameters studied in this work, could be performed. This work can also be expanded to include different surface types, such as porous surfaces, to determine the relationships between skewness and kurtosis and the surface roughness.

Bibliography

- [1] Karl Pearson. Contributions to the mathematical theory of evolution. *Philosophical Transactions of the Royal Society of London. A*, 185:71–110, 1894.
- [2] Karl Pearson. Contributions to the mathematical theory of evolution. II. skew variation in homogeneous material. *Philosophical Transactions of the Royal Society of London. A*, 186:343–414, 1895.
- [3] Anna M. Fiori and Michele Zenga. Karl Pearson and the origin of kurtosis. *International Statistical Review*, 77 (1):40–50, 2009.
- [4] L.M. Lesser. Letter to the editor. *Journal of Statistics Education*, 13 (2), 2005.
- [5] A.L. Bowley. *Elements of Statistics*. Scribner, New York, 1920.
- [6] Karl Pearson. V. On the mathematical theory of errors of judgement, with special reference to the personal equation. *Philosophical Transactions of the*

-
- Royal Society of London. A*, 60:236–299, 1902.
- [7] E.S. Gadelmawla, M.M. Koura, T.M.A. Maksoud, L.M. Elewa, and H.H. Soliman. Roughness parameters. *Journal of Materials Processing Technology*, 123:133–145, 2002.
- [8] Jouko Peltonen, Mikael Järn, Sami Areva, Mike Linden, and Jarl B. Rosenholm. Topographical parameters for specifying a three-dimensional surface. *American Chemical Society*, 20:9428–9431, 2004.
- [9] Marko Sedlaček, Luis Miguel Silva Vilhena, Bojan Podgornik, and Jože Vižintin. Surface topography modelling for reduced friction. *Journal of Mechanical Engineering*, 57:674–680, 2011.
- [10] Marko Sedlaček, Bojan Podgornik, and Jože Vižintin. Correlation between standard roughness parameters skewness and kurtosis and tribological behaviour of contact surfaces. *Tribology International*, 48:102–112, 2012.
- [11] Nouredine Tayebi and Andreas A. Polycarpou. Modelling the effect of skewness and kurtosis on the static friction coefficient of rough surfaces. *Tribology International*, 37:491–505, 2004.
-

-
- [12] Karl Niklas Hansson and Stig Hansson. Skewness and kurtosis: Important parameters in the characterization of dental implant surface roughness-A computer simulation. *International Scholarly Research Network Materials Science*, 2011, 2011.
- [13] Agnes Batista Meireles, Flavia de Souza Bastos, Tulimar Pereira Cornacchia, Janaina Alvernaz Ferreria, and Estevam Barbosa de Las Casas. Enamel wear characterization based on a skewness and kurtosis surface roughness evaluation. *Biotribology*, 2015.
- [14] W. Wang, H. Chen, Y. Hu, and H. Wang. Effect of surface roughness parameters on mixed lubrication characteristics. *Tribology International*, 39:522–527, 2006.
- [15] Berrin İközler and Sümer M. Perker. Effect of the seed layer thickness on the stability of ZnO nanorod arrays. *Thin Solid Films*, 558:149–159, 2014.
- [16] P. Martin. Correlating surface roughness to the root mean squared roughness, skewness and kurtosis., 4 2012.
- [17] W.B. Yuan, T.V. Vorburger, J.F. Song, and T.B. Renegar. A simplified realization for the gaussian filter in surface metrology. *X International Colloquium on Surfaces*, page 133, 2000.
-

-
- [18] G. Farin and D Hansford. *Practical Linear Algebra: A Geometry Toolbox*. A. K. Peters, Ltd., 888 Worcester Street, Suite 230, Wellesley, MA, 2004.
- [19] David W. Scott. On optimal and data-based histograms. *Biometrika*, 66 (3):605–610, 1979.
- [20] R.L. Alley, K. Komvopoulos, and R.T. Howe. Self-assembled monolayer film for enhanced imaging of rough surfaces with atomic force microscopy. *Journal of Applied Physics*, 76 (10):5731–5737, 1994.
- [21] R.A. Fisher. Moments and product moments of sampling distributions. *Proceedings of the London Mathematical Society*, pages 199–238, 1928.
- [22] R.A. Fisher. The moments of the distribution for normal samples of departure from normality. *Proceedings of the Royal Society of London. Series A, Containing Papers of a Mathematical and Physical Character*, 130 (812):16–28, 1930.
- [23] X. Jane Xiang and David J. Whitehouse. Technological shifts in surface metrology. *CIRP Annals Manufacturing Technology*, 61:815–836, 2012.
- [24] X. Liu, D.G. Chetwynd, and J.W. Gardner. Surface characterisation of electroactive thin polymeric film bearings. *International Journal of Machine Tools and Manufacture*, 38 (5-6):669–675, 1998.
-

-
- [25] Karl Pearson. Mathematical contributions to the theory of evolution.-IX. On the principle of homotyposis and its relation to heredity, to the variability of the individual, and to that of race. Part I.-Homotyposis in the vegetable kingdom. *Philosophical Transactions of the Royal Society of London. A*, 1901.
- [26] Karl Pearson. Das fehlergesetz und seine verallgemeinerungen durch Fechner und Pearson. A rejoinder. *Biometrika Trust*, 4:169–212, 1905.
- [27] Richard J. Pike and Tom R. Thomas. Quantitative characterization of microtopography- a bibliography of industrial surface metrology. *U.S. Geological Survey*, 1998.
- [28] T.R. Thomas. Characterization of surface roughness. *Precision Engineering*, 3 (2):97–104, 1981.
-